Supplementary Information for:

Engineering a molecular electrocatalytic system for energy-efficient ammonia production from wastewater nitrate

Dean M. Miller[1], Matthew J. Liu[1], Kristen Abels[1], Anna Kogler[2], Kindle S. Williams,[1] William A. Tarpeh[1,2,3,*]

[1]Department of Chemical Engineering, Stanford University, Stanford, CA, 94305, United States

[2]Department of Civil and Environmental Engineering, Stanford University, Stanford, CA, 94305, United States

[3]Woods Institute for the Environment, Stanford University, Stanford, California 94305, United States

*Corresponding author, Email: wtarpeh@stanford.edu. Address: 443 Via Ortega, Room 387, Stanford CA, 94305, USA. Telephone: (650) 497-1324

65 pages

7 tables

39 figures

44 equations

Submitted to: *Energy & Environmental Science*

47

Section S1: Catalyst and wastewater characterization

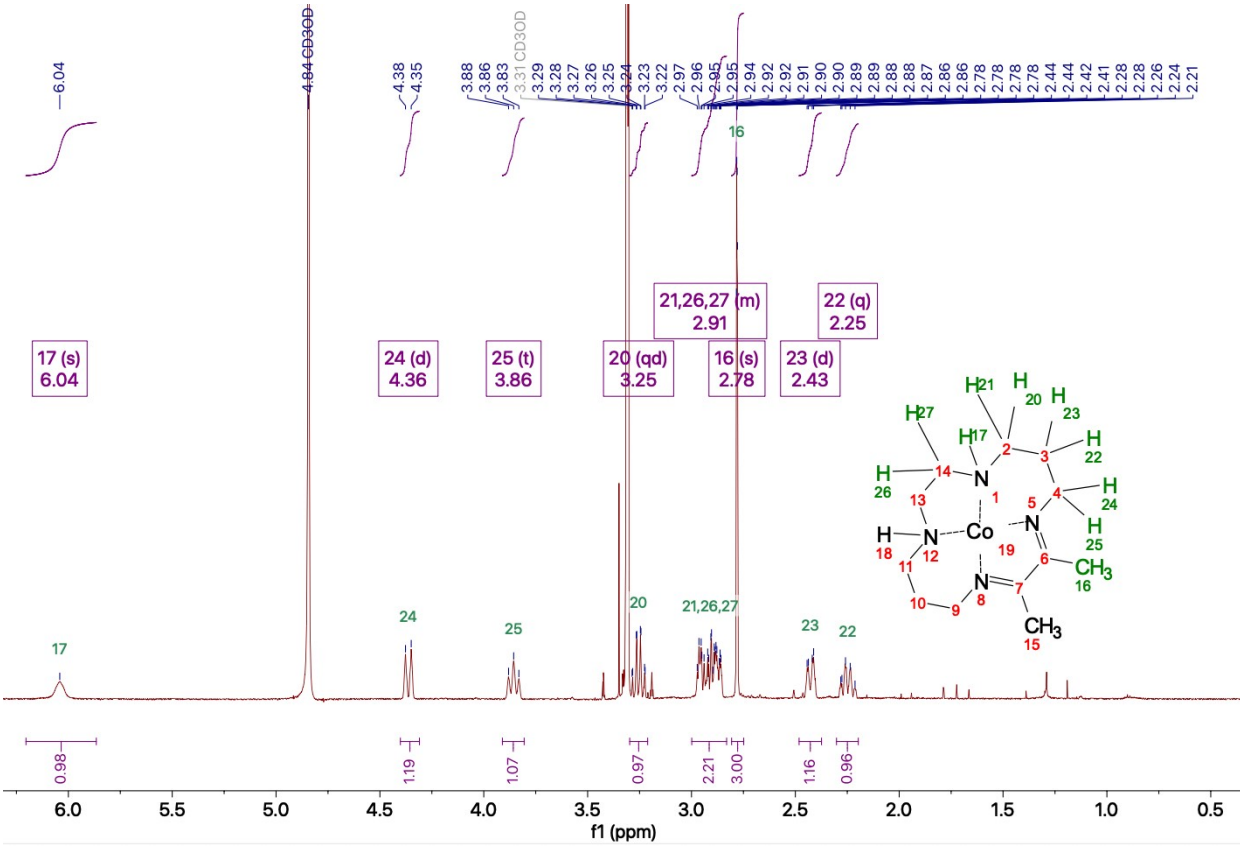

Fig. S1. ^{1}H NMR of Co(DIM) in CD_3OD (deuterated methanol).

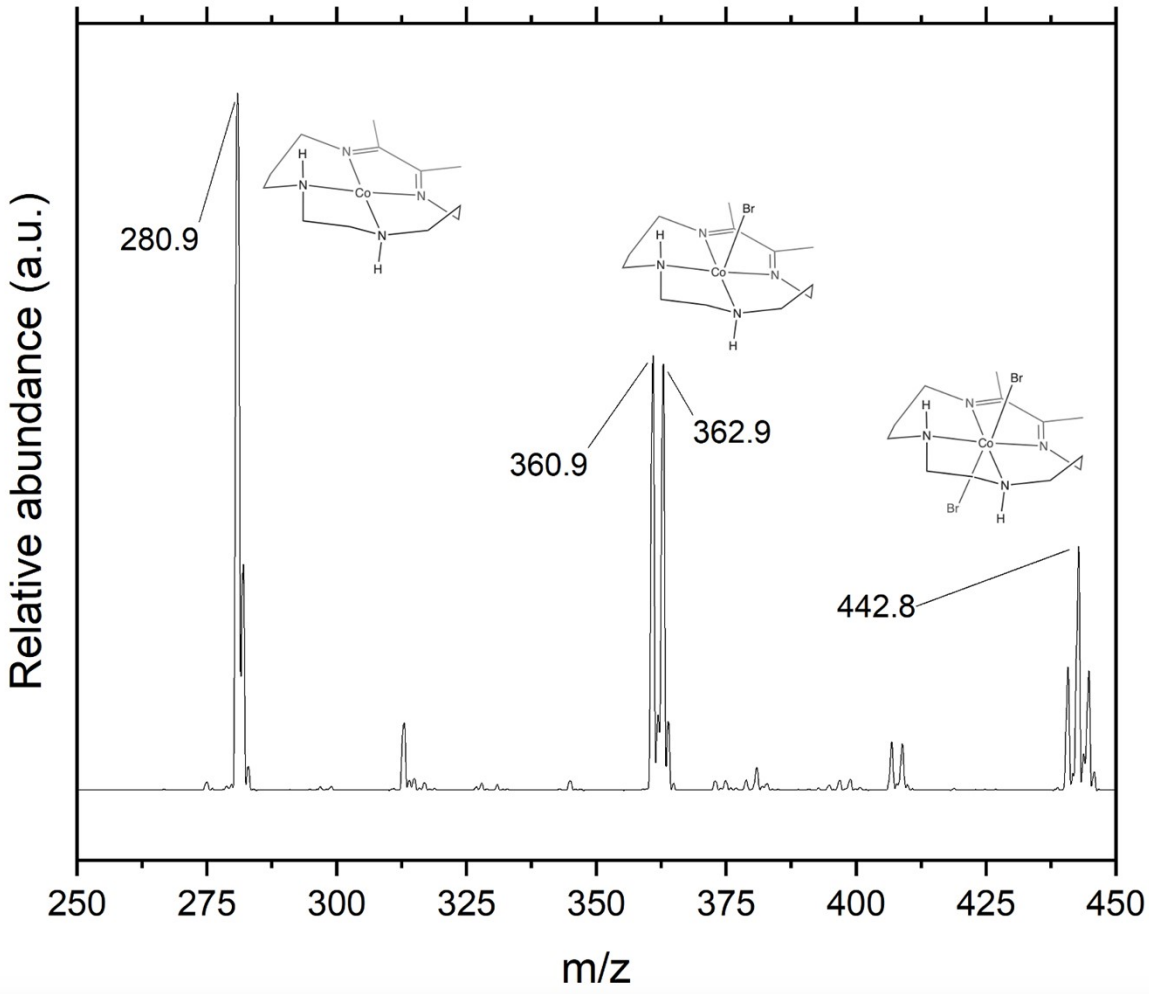

Fig. S2. Mass spectra for aqueous Co(DIM). Co(DIM) samples were prepared for high performance liquid chromatography-mass spectrometry (HPLC-MS) analysis by diluting 1 mg/mL aqueous solutions by a factor of 5 using a methanol/water mixture (50:50 v/v). Samples were analyzed via direct injection on an Agilent 1260 HPLC with an Agilent 6460 Triple Quadrupole MS (Agilent, Santa Clara, CA). Samples were eluted using 98% aqueous mobile phase (0.1% formic acid) and 2% organic mobile phase (acetonitrile) at a flowrate of 0.6 mL/min. 10 µL of sample were injected during each run. Compounds were detected using positive electrospray ionization mode with a gas temperature of 300 ºC, gas flowrate of 7 L/min, a nebulizer pressure of 45 psi, a sheath gas temperature of 250 ºC, a sheath gas flowrate of 9 L/min, a capillary voltage of 3500 V, a nozzle voltage of 500 V, a fragmentor energy of 50 V, and a cell accelerator voltage of 7 V.

LC-MS fragment weights match reasonably well with the molecular weight of Co(DIM) bound to zero Br^- ions (283.29), one Br^- ion (363.19), and two Br^- ions (443.09). Additionally, ^{79}Br and ^{81}Br exist in roughly equal parts naturally at standard temperature and pressure, causing the spectra to exhibit a triplet at 442.8 m/z, a doublet at 361.9 m/z, and a singlet at 280.9 m/z.

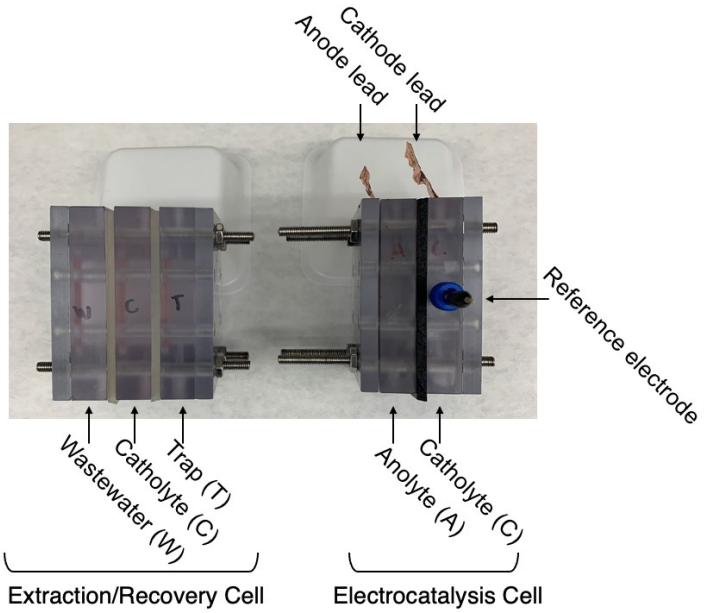

67

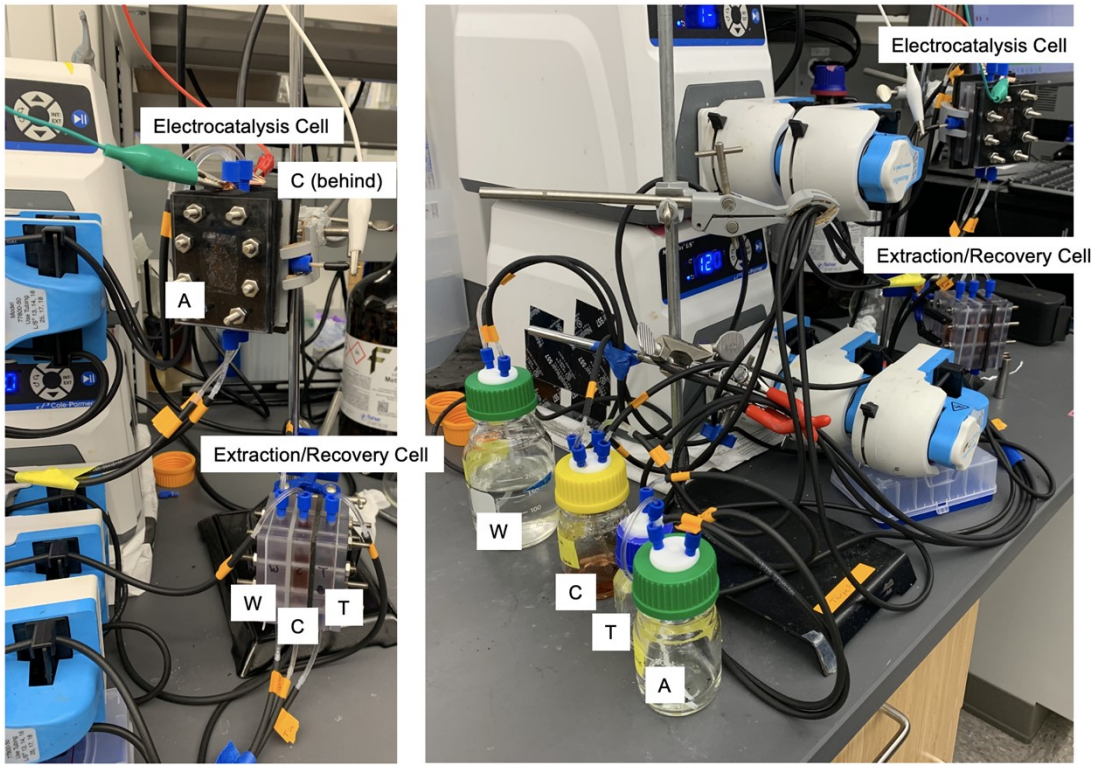

68

69 Fig. S3. Photos of electrocatalyst-in-a-box (ECaB) reactor. Top photo: ECaB reactor profile before being
70 plumbed with recirculation tubing. Bottom left photo: three-chamber extraction/recovery cell (bottom),
71 two-chamber electrocatalysis reactor (top). Bottom right photo: flow setup showing reactor system, pumps,
72 and batch recirculation bottles.

Table S1. Simplified, simulated, and real wastewater characterization.

Species*	Simplified Wastewater	Simulated Wastewater	Real Wastewater
Nitrate	28 mg-N/L	28 mg-N/L	28 mg-N/L
Chloride	217 mg/L	242 mg/L	228 mg/L
Bicarbonate	-	84 mg/L	79 mg/L
Sulfate	-	106 mg/L	102 mg/L
Sodium	52.2 mg/L	120 mg/L	120 mg/L
Potassium	-	20 mg/L	20 mg/L
Magnesium	-	36 mg/L	36 mg/L
Calcium	-	76 mg/L	77 mg/L
pH (without 8 mM Co(DIM))	6.50	8.55	8.30
pH (with 8 mM Co(DIM))	3.06	3.42	3.58

*Fluoride, nitrite, bromide, phosphate, and lithium were measures but not detected in the real wastewater by ion chromatography.

Section S2: Cyclic voltammetry (CV)

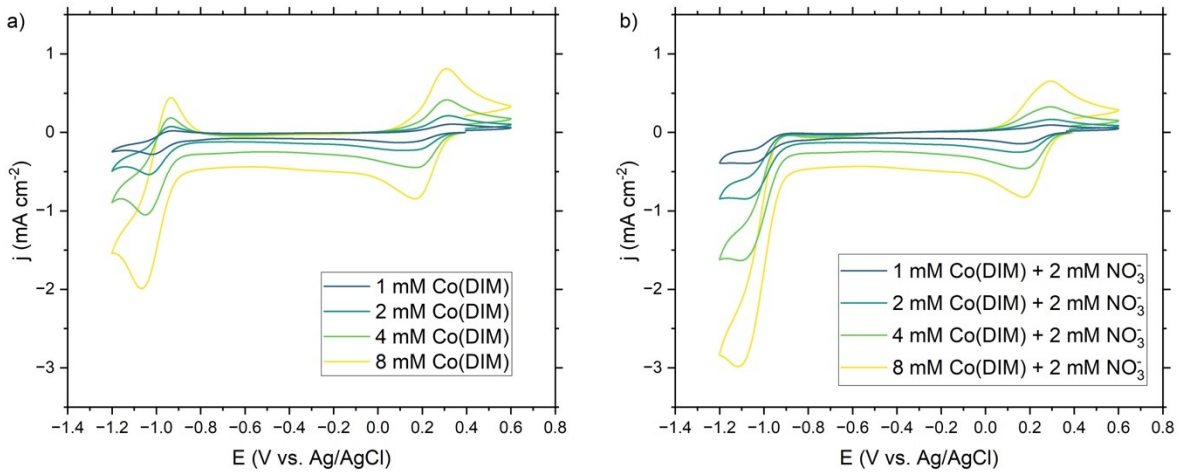

Fig. S4. a) CVs as a function of [Co(DIM)] in the absence of nitrate. b) CVs as a function of Co(DIM) with 2 mM nitrate (2 mM $NaNO_3$). Working electrode: 5 mm GC disk. Counter electrode: 6.6 mm graphite rod. Reference electrode: Ag/AgCl (4.0 M KCl). Background electrolyte: 6.2 mM NaCl.

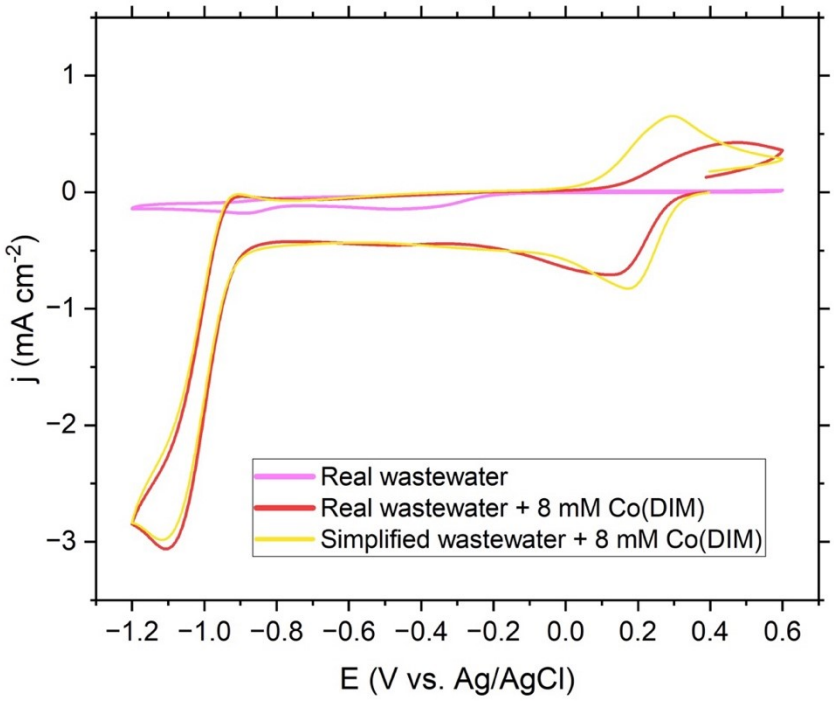

83

84 Fig. S5. CVs of 8 mM Co(DIM) in real secondary effluent wastewater and in simplified wastewater (6.2

85 mM NaCl + 2 mM $NaNO_3$) for comparison. Working electrode: 5 mm GC disk. Counter electrode: 6.6 mm

86 graphite rod. Reference electrode: Ag/AgCl (4.0 M KCl).

87

Section S3: Controlled-potential electrolysis (CPE)

Section S3.1: Equations used to evaluate CPEs

$$S_{TAN} = \frac{mol\ TAN_{produced}}{mol\ NO_3^-(initial) - mol\ NO_3^-(t)} \quad \text{(Equation S3.1.1)}$$

$$FE\ to\ TAN\ (\%) = \left(\frac{n * F *\ mol\ TAN_{produced}}{Q_{passed}}\right) * 100\% \quad \text{(Equation S3.1.2)}$$

where

n = number of electrons required to produce one mole of TAN from NO_3^-, Q_{passed} = charge p

and $F = 96485\ C\ mol^{-1}$

$$X_{NO_3^-}(t) = \frac{mol\ NO_3^-(initial) - mol\ NO_3^-(t)}{mol\ NO_3^-(initial)} \quad \text{(Equation S3.1.3)}$$

Section S3.2: Aqueous characterization of CPE experiments

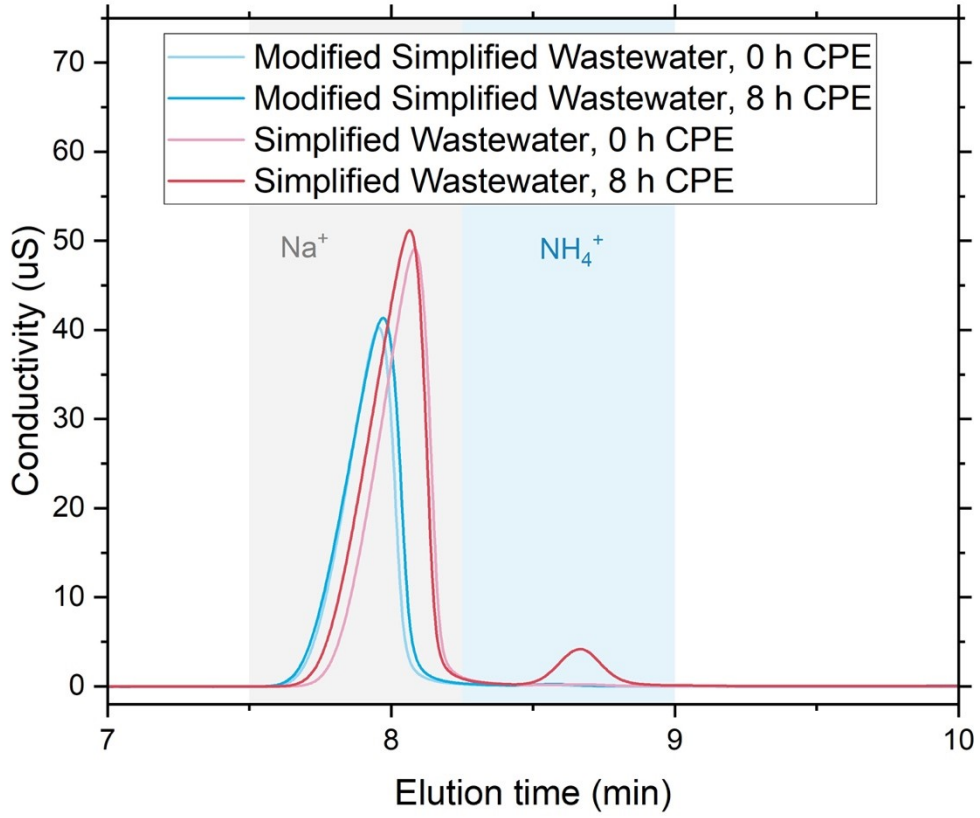

Fig. S6. Cation chromatograms of aqueous samples from CPEs in modified simplified wastewater (8 mM Co(DIM) + 6.2 mM NaCl) and in simplified wastewater (8 mM Co(DIM) + 6.2 mM NaCl + 2 mM $NaNO_3$).

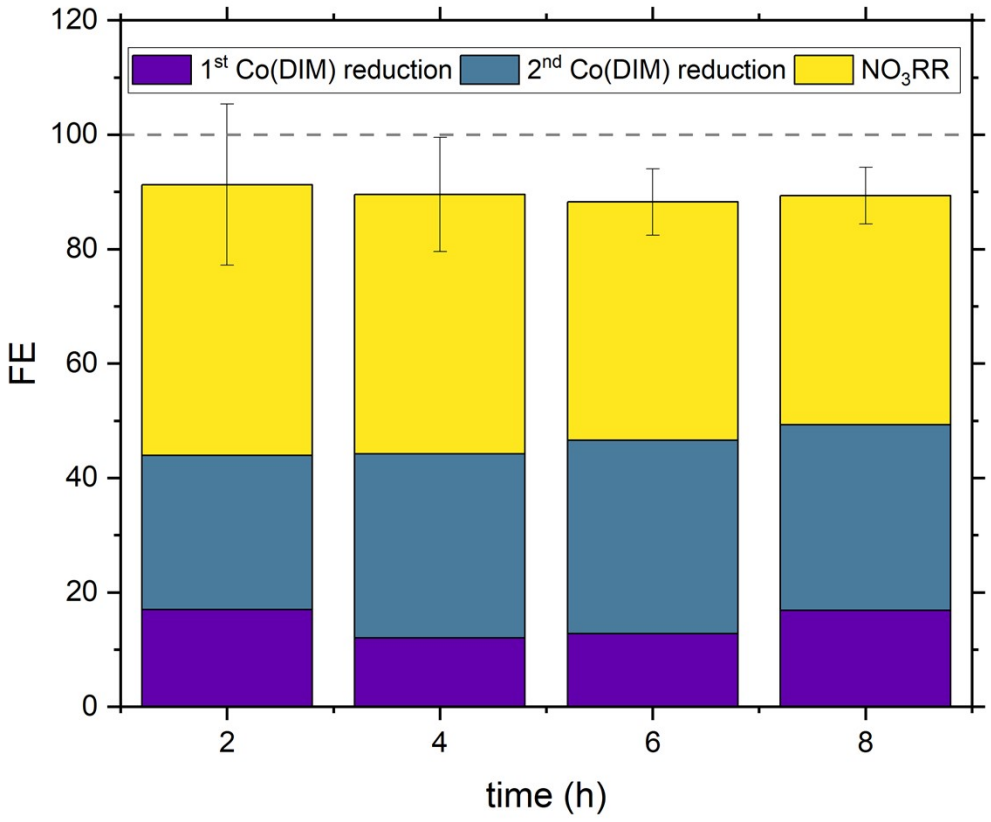

Fig. S7. Charge decomposition into the first Co(DIM) reduction, second Co(DIM) reductions, and NO_3RR. –1.05 V vs. Ag/AgCl applied for NO_3RR (yellow; simplified wastewater: 8 mM Co(DIM) + 6.2 mM NaCl + 2 mM $NaNO_3$) and 2nd Co(DIM) reduction (green; modified simplified wastewater: 8 mM Co(DIM) + 6.2 mM NaCl). –0.75V vs. Ag/AgCl (–0.99 V vs. first reduction, +0.25 V vs. second reduction) applied for 1st Co(DIM) reduction (purple; simplified wastewater: 8 mM Co(DIM) + 6.2 mM NaCl + 2 mM $NaNO_3$). Error bars represent ± one standard deviation from triplicate experiments (n=3) for NO_3RR experiments (yellow; simplified wastewater: 8 mM Co(DIM) + 6.2 mM NaCl + 2 mM $NaNO_3$). The CPE experiments to quantify charge associated with non-catalytic 1st and 2nd reductions of Co(DIM) were only performed once because no conversion of nitrate and no production of TAN was observed.

Section S3.3: Post CPE characterization

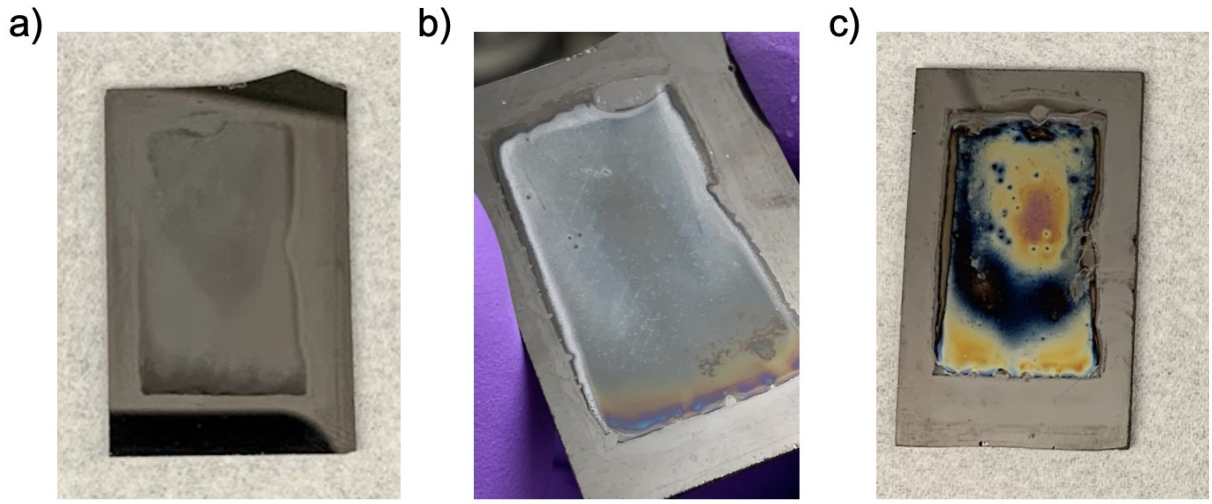

Fig. S8. Photos of GC cathodes post CPE in (a) simplified, (b) simulated, and (c) real wastewater. –1.05 V vs. Ag/AgCl was held for 8 hours, then the cathode was removed, rinsed thoroughly with water, and blown dry with N_2. The anode was a 5.4 cm^2 MMO electrode. Leakless Ag/AgCl (3.4 M KCl) reference electrode. Cathode and anode chambers were separated by a CEM.

120 Table S2. Possible precipitates from real secondary effluent wastewater.

Possible precipitate	Concentration of relevant ions in real wastewater	K_{sp} of precipitate[1]
$Mg(OH)_2$	$[Mg^{2+}] = 1.5$ mM $[OH^-]_{RDL} = 10^{-(14 - pH_{RDL})}$	5.61×10^{-12}
$MgCO_3$	$[Mg^{2+}] = 1.5$ mM $[HCO_3^-] = 1.4$ mM $[CO_3^{2-}]_{RDL} = \frac{[HCO_3^-] \times 10^{-pKa_{HCO_3^-/CO_3^{2-}}}}{10^{-pH_{RDL}}}$; $pKa_{HCO_3^-/CO_3^{2-}} = 10.3$	6.82×10^{-6}
$MgSO_4 \cdot 7H_2O$	$[Mg^{2+}] = 1.5$ mM $[SO_4^{2-}] = 1.1$ mM	*n.a..* *(soluble in water up to 1.1 kg/L)*
$Ca(OH)_2$	$[Ca^{2+}] = 1.9$ mM $[OH^-]_{RDL} = 10^{-(14 - pH_{RDL})}$	5.02×10^{-6}
$CaCO_3$	$[Ca^{2+}] = 1.9$ mM $[HCO_3^-] = 1.4$ mM $[CO_3^{2-}]_{RDL} = \frac{[HCO_3^-] \times 10^{-pKa_{HCO_3^-/CO_3^{2-}}}}{10^{-pH_{RDL}}}$; $pKa_{HCO_3^-/CO_3^{2-}} = 10.3$	3.36×10^{-9}*
$CaSO_4 \cdot 2H_2O$	$[Mg^{2+}] = 1.5$ mM	3.14×10^{-5}

	$[SO_4^{2-}]$ = 1.1 mM	

*K_{sp} shown for $CaCO_3$ corresponds to calcite, which has the lowest K_{sp} among possible precipitates.

To determine the interfacial pH required for precipitation of $Mg(OH_2)$ we began by setting the solubility product quotient (Q_{sp}) equal to the solubility product constant (K_{sp}).

$$Q_{sp} = [Mg^{2+}][OH^-]^2 = K_{sp} = 5.61 \times 10^{-12} \quad \text{(Equation S3.3.1)}$$

Plugging in $[Mg^{2+}]$ = 1.5 mM and solving for [OH^-] yields the pH necessary for precipitation of $Mg(OH)_2$ in the RDL: pH_{RDL} = 9.8. The same procedure was used to determine the necessary pH for precipitation of $Ca(OH)_2$: pH_{RDL} = 12.8.

Determining the interfacial pH required for precipitation of carbonates like $MgCO_3$ is only slightly more complex because of the HCO_3^-/CO_3^{2-} acid/base pair, where magnesium and calcium bicarbonate are significantly more soluble than their carbonate analogues. We again set Q_{sp} equal to K_{sp}.

$$Q_{sp} = [Mg^{2+}][CO_3^{2-}] = K_{sp} = 6.82 \times 10^{-6} \quad \text{(Equation S3.3.2)}$$

Plugging in $[Mg^{2+}]$ = 1.5 mM and solving for $[CO_3^{2-}]$ yields the $[CO_3^{2-}]$ necessary for precipitation of $MgCO_3$ in the RDL: 4.5 mM. This concentration is greater than the 1.4 mM bicarbonate in bulk solution, making precipitation of $MgCO_3$ unlikely. We performed the same procedure for $CaCO_3$.

$$Q_{sp} = [Ca^{2+}][CO_3^{2-}] = K_{sp} = 3.36 \times 10^{-9} \quad \text{(Equation S3.3.3)}$$

Precipitation of $CaCO_3$ is possible because the $[CO_3^{2-}]$ necessary is 1.8 μM. Because the bulk pH of the Real Wastewater was 8.30 << $pKa_{HCO_3^-/CO_3^{2-}} = 10.3$, the majority of inorganic carbon in bulk solution exists as bicarbonate. The concentration of carbonate is therefore dependent on the RDL pH assuming the acid/base pair is equilibrated by rapid proton transfer kinetics.

$$10^{-pKa_{HCO_3^-/CO_3^{2-}}} = \frac{[CO_3^{2-}]_{RDL} \times 10^{-pH_{RDL}}}{[HCO_3^-]_{RDL}} \quad \text{(Equation S3.3.4)}$$

$$10^{-pH_{RDL}} = \frac{10^{-pKa_{HCO_3^-/CO_3^{2-}}} \times \left[HCO_3^-\right]_{RDL}}{\left[CO_3^{2-}\right]_{RDL}} \quad \text{(Equation S3.3.5)}$$

$$pH_{RDL} = -\log\left(\frac{10^{-pKa_{HCO_3^-/CO_3^{2-}}} \times \left[HCO_3^-\right]_{RDL}}{\left[CO_3^{2-}\right]_{RDL}}\right) \quad \text{(Equation S3.3.6)}$$

The unknown $\left[HCO_3^-\right]_{RDL}$ can be eliminated by a mass balance of bicarbonate and carbonate.

$$pH_{RDL} = -\log\left(\frac{10^{-pKa_{HCO_3^-/CO_3^{2-}}} \times \left(1.4\ mM - \left[CO_3^{2-}\right]_{RDL}\right)}{\left[CO_3^{2-}\right]_{RDL}}\right) \quad \text{(Equation S3.3.7)}$$

Plugging in $\left[CO_3^{2-}\right]_{RDL}$= 1.8 μM, the RDL pH necessary for precipitation of $CaCO_3$ is 4.4 which is less than the pH of the bulk solution. Complex aqueous solutions like the real wastewater in this study are nevertheless able to keep Ca^{2+} and HCO_3^- solvated in bulk solution.[2] We hypothesize that interfacial coulombic effects in Co(DIM)-mediated NO_3RR prevented $CaCO_3$ deposition and may explain why we did not see a strong signal for calcium in XPS or EDS for any GC cathode analyzed. One such effect could be Co(DIM) axially coordinating bicarbonate/carbonate,[3] precluding deposition.

Finally, precipitation of magnesium as a sulfate is unlikely because the hydrate ($MgSO_4 \cdot 7H_2O$) is soluble in mass fractions greater than 1:1 with water. Precipitation of $CaSO_4 \cdot 2H_2O$ is also unlikely because the concentration of sulfate necessary (16.5 mM) exceeds the concentration in the real wastewater (1.1 mM), as shown by setting Q_{sp} equal to K_{sp} in Equation S3.3.8.

$$Q_{sp} = \left[Ca^{2+}\right]\left[SO_4^{2-}\right] = K_{sp} = 3.14 \times 10^{-5} \quad \text{(Equation S3.3.8)}$$

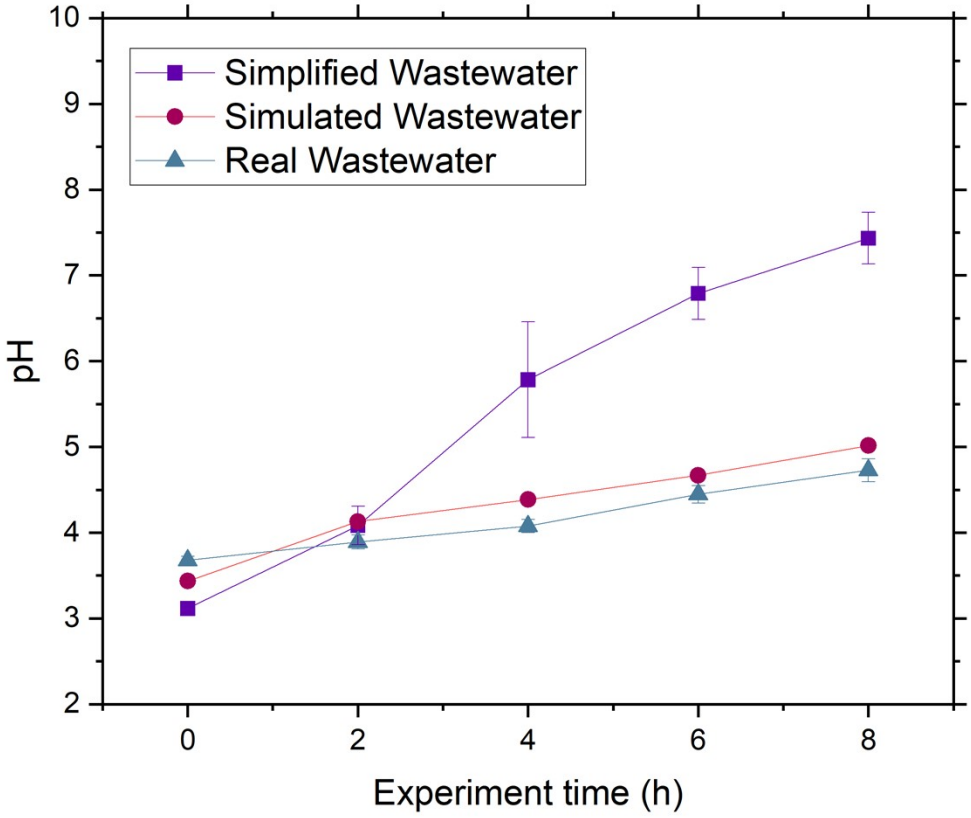

Fig. S9. pH trends of 2-chamber CPEs as a function of time. Error bars represent ± one standard deviation from triplicate experiments (n=3). Error bars not shown are smaller than the symbol.

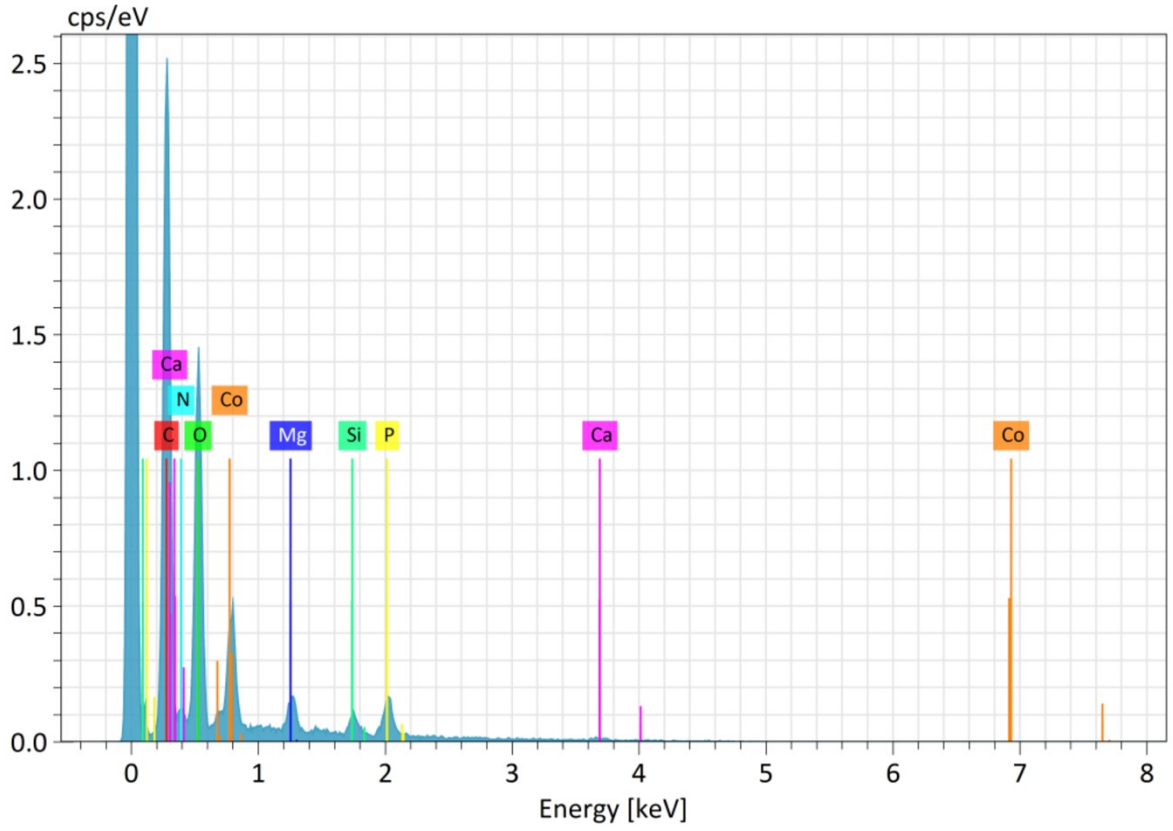

162

163 Fig. S10. EDS spectra of GC cathode post CPE in real wastewater.

164

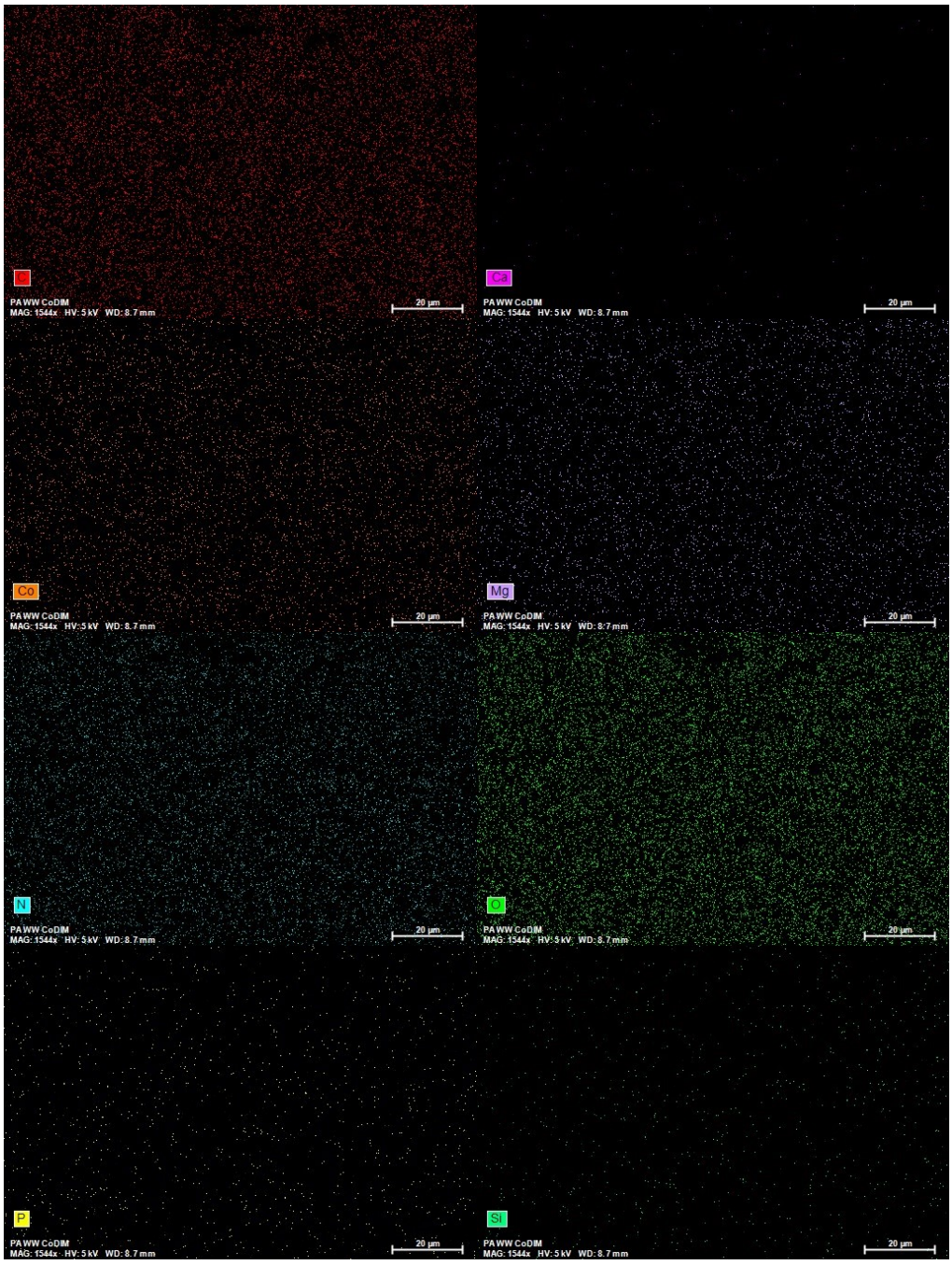

Fig. S11. EDS dark field maps of C, Ca, Co, Mg, N, O, P, and Si on GC electrodes post real wastewater CPE.

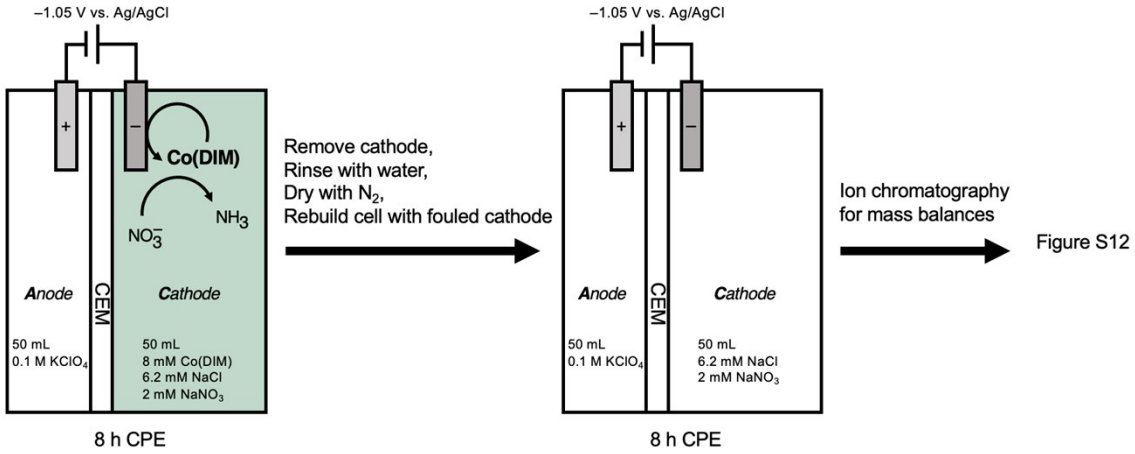

172

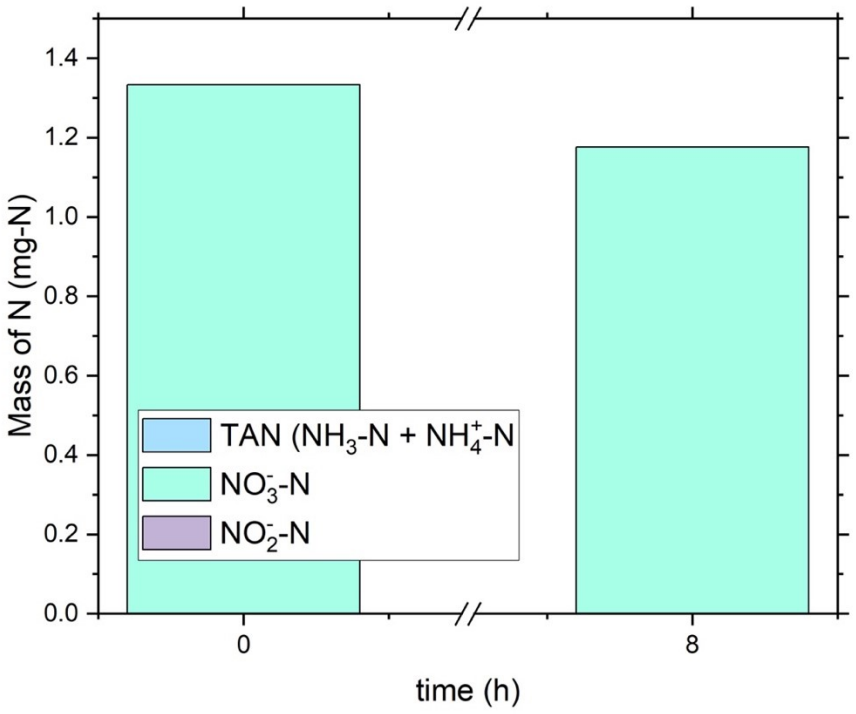

173

174 Fig. S12. Nitrogen mass balances for the rinse test (in simplified wastewater) of the deposit formed in {8

175 mM Co(DIM) + simplified wastewater}. No TAN or $^{NO_2^-}$ was detected by ion chromatography. Detection

176 limit for $^{NO_3^-}$: 1.0 mg-$^{NO_3^-}$/L. Detection limit for $^{NO_2^-}$: 1.0 mg-$^{NO_2^-}$/L. Detection limit for TAN: 0.25 mg

177 $^{NH_4^+}$/L.

178

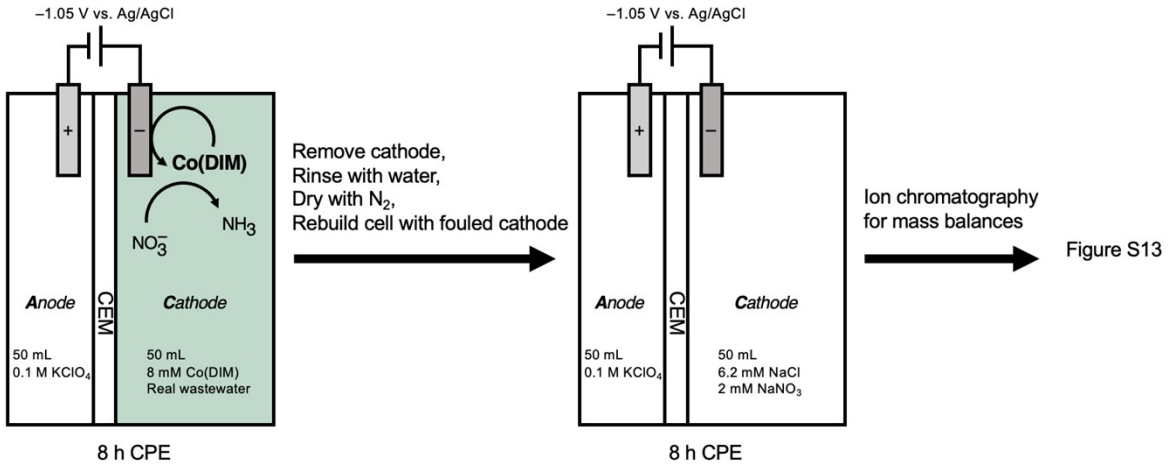

179

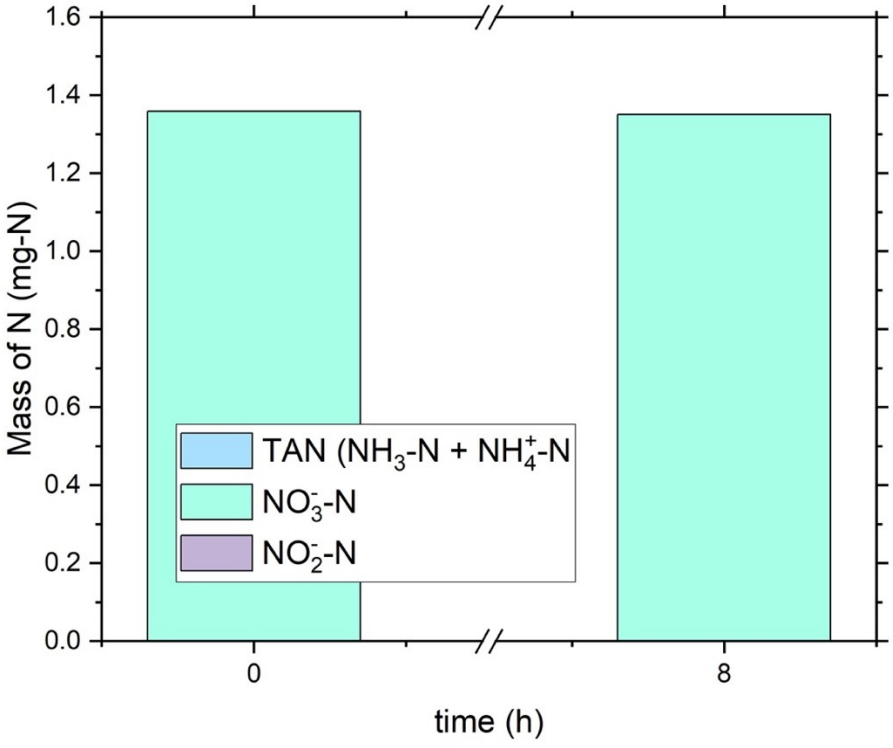

180

181 Fig. S13. N mass balances for the rinse test (in simplified wastewater) of the deposit formed in {8 mM

182 Co(DIM) + real wastewater}. No TAN or NO_2^- was detected by ion chromatography. Detection limit for

183 NO_3^-: 1.0 mg-NO_3^-/L. Detection limit for NO_2^-: 1.0 mg-NO_2^-/L. Detection limit for TAN: 0.25 mg NH_4^+/L.

184

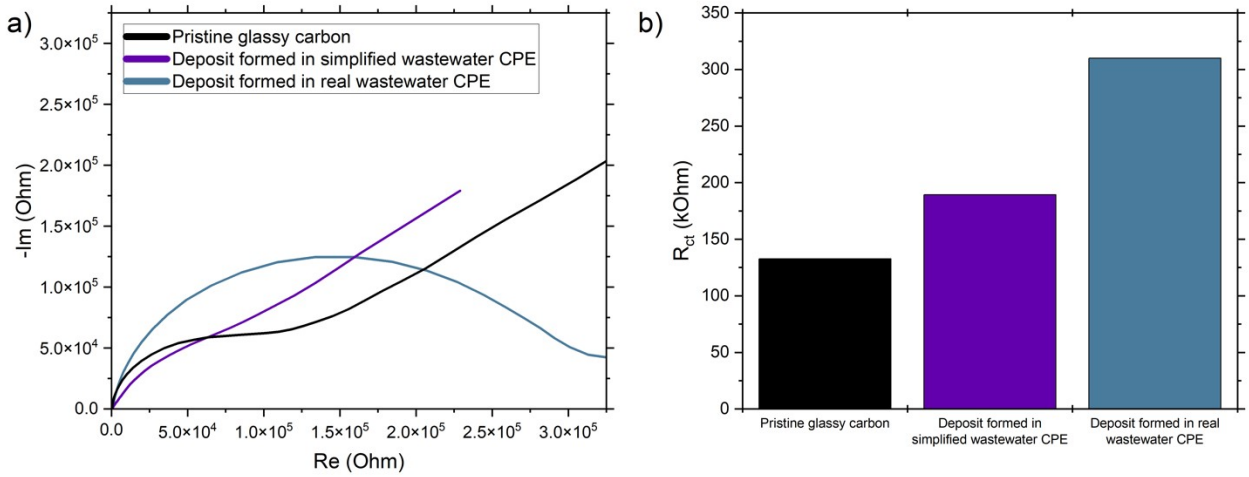

185

186 Fig. S14. a) Nyquist plots for potentiostatic electrochemical impedance spectroscopy (PEIS) of deposits
187 formed in CPE. The electrolyte was 8 mM Co(DIM) + 6.2 mM NaCl + 2 mM $NaNO_3$ and the measurement
188 was performed at open circuit with a sinusoidal potential amplitude of 10 mV and a frequency range of 1
189 MHz to 10 mHz. An electrochemical cone cell was used with a circular working electrode opening 5 mm
190 in diameter. The counter electrode was a 6.4 mm graphite rod and the reference electrode was a Ag/AgCl
191 (4.0 M KCl) electrode. R_{ct} was calculated by fitting a semi-circle to the region of the Nyquist plot before
192 the Warburg, then subtracting R_u (the low x-intercept of the Nyquist plot) from R_{ct} + R_u (the high x-
193 intercept).[4,5] b) Measured R_{ct} values from PEIS.

194

Section S4: Transport and contaminant conditions for catalysis inhibition

Section S4.1: Rotating disk electrode

To interrogate the sensitivity of inhibition to interfacial electrolyte composition, we used a rotating-disk electrode (RDE) to achieve well-defined transport conditions in the RDL. By varying the rotation rate, we modulated the delivery rate (and therefore steady-state concentrations) of NO_3^-, Co(DIM), and wastewater constituents during CPE. Under stagnant conditions (0 rotations per minute (RPM)), the current density of Co(DIM)-mediated NO_3RR in simplified wastewater (2 mM NO_3^-) was greater than that of Co(DIM) in simplified wastewater (0 mM NO_3^-), demonstrating steady-state catalytic current (Fig. 3a). Catalytic current in simplified wastewater was also observed with rotation rates of 9 and 25 RPM, indicating that homogeneous NO_3RR outpaces bulk catalyst delivery to the electrode surface with modest forced convection.[6] Conversely, catalytic current is lost in the range of 100 to 400 RPM, indicating that bulk catalyst delivery outpaces NO_3RR (Fig. S15). The rotation rates tested therefore span transport conditions for Co(DIM)-mediated NO_3RR catalysis and for Co(DIM) activation with no catalysis. In real wastewater (2 mM NO_3^-), the current density vs. time effectively overlays with the simplified wastewater (2 mM NO_3^-) for the duration of the 5 min CPE, indicating no inhibition under stagnant conditions. Disturbing the RDL by forced convection causes a decay in current density in real wastewater, indicating inhibition. The coupled transport conditions and bulk solution composition for a fixed electrode potential therefore describe inhibition conditions.

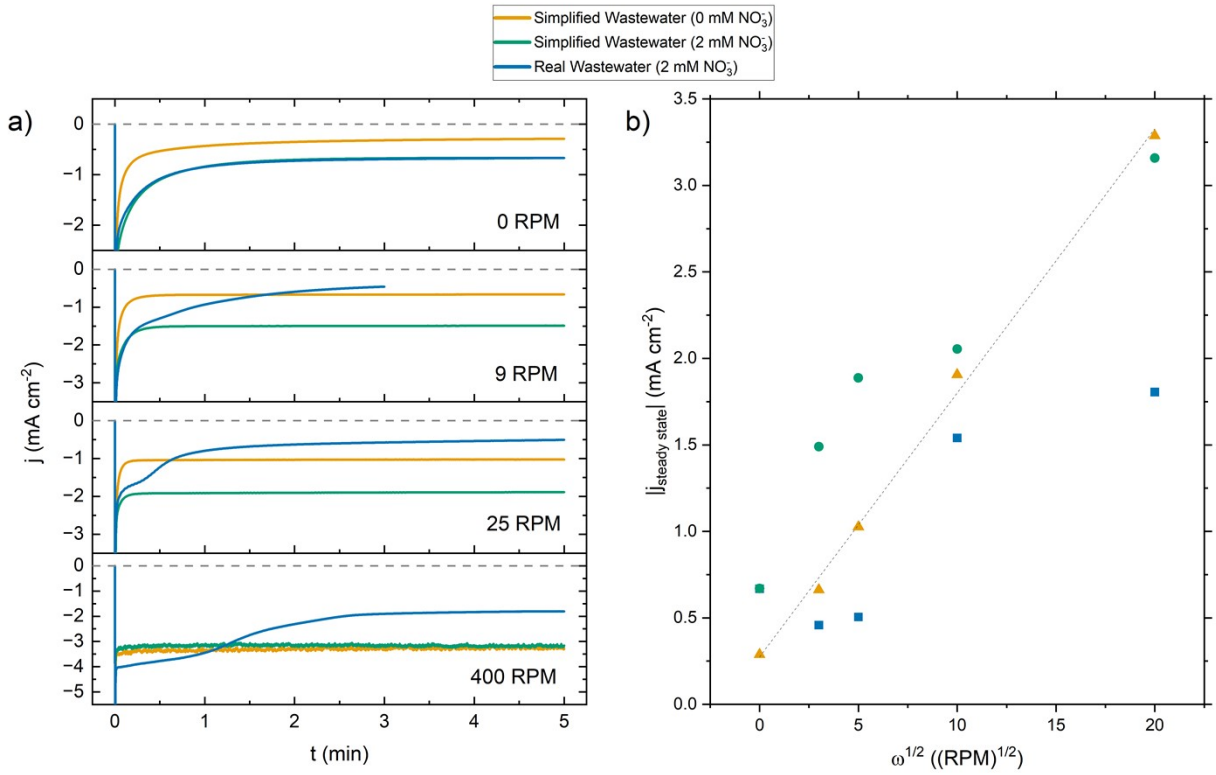

Fig. S15. **(**a) Current density vs. time for controlled-potential electrolysis (CPE) at –1.05 V vs. Ag/AgCl performed in a rotating-disk electrode (RDE) setup with 8 mM Co(DIM) as a function of rotations per minute (RPM) in three electrolyte: simplified wastewater (0 mM NO_3^-), simplified wastewater (2 mM NO_3^-), and real wastewater(2 mM NO_3^-). The controlled rotation rate varied the delivery of NO_3^-, Co(DIM), and wastewater constitutents to the RDL while the current density was monitored as a proxy for the NO_3RR activity. Rotation rates were kept below 400 RPM because faster rotation rates resulted in loss of catalytic current (i.e., the same current density was observed for simplified wastewater (0 mM NO_3^-) and simplified wastewater (2 mM NO_3^-)). b) Steady-state currents of RDE CPEs from Fig. 3a plotted versus the square root of rotation rate (a proxy for diffusion layer thickness[5]). In the presence of nitrate and under sufficiently fast rotation rates, bulk catalyst delivery outpaces NO_3RR, causing the green and blue points to be nonlinear.

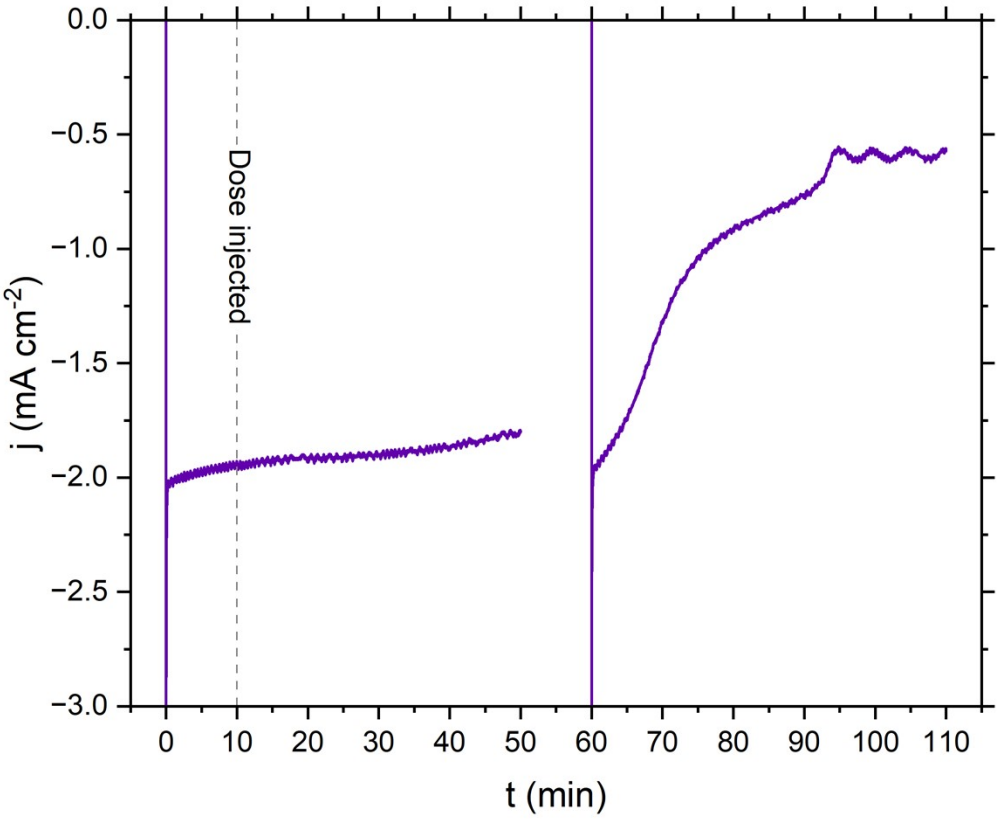

226

227 Fig. S16. Chronoamperogram for longer Mg dose RDE CPE experiment. –1.05 $V_{Ag/AgCl}$ was applied from
228 t = 0 to 50 minutes. 28 µL of 1 M $MgCl_2$ was injected into the electrolyte at t = 10 min. Then a period of
229 open circuit potential (OCP) was held from t = 50 min to 60 min. Finally, –1.05 $V_{Ag/AgCl}$ was applied from
230 t = 60 to 110 minutes.

Section S4.2: Two-chamber CPE contaminant dosing experiments

In contaminant dosing experiments, the same two-chamber CPE setup was used as described in Materials & Methods 2.2.2. After the 2 h sample aliquots were drawn from cathode and anode chambers, a small volume of 1 M salts were manually injected (70 µL 1 M $MgCl_2$, 75 µL 1 M $NaHCO_3$, 95 µL 1 M $CaCl_2$) into the catholyte recirculation bottle. The volume was chosen such that the catholyte concentration of the target contaminant matched the target contaminant concentration in real wastewater.

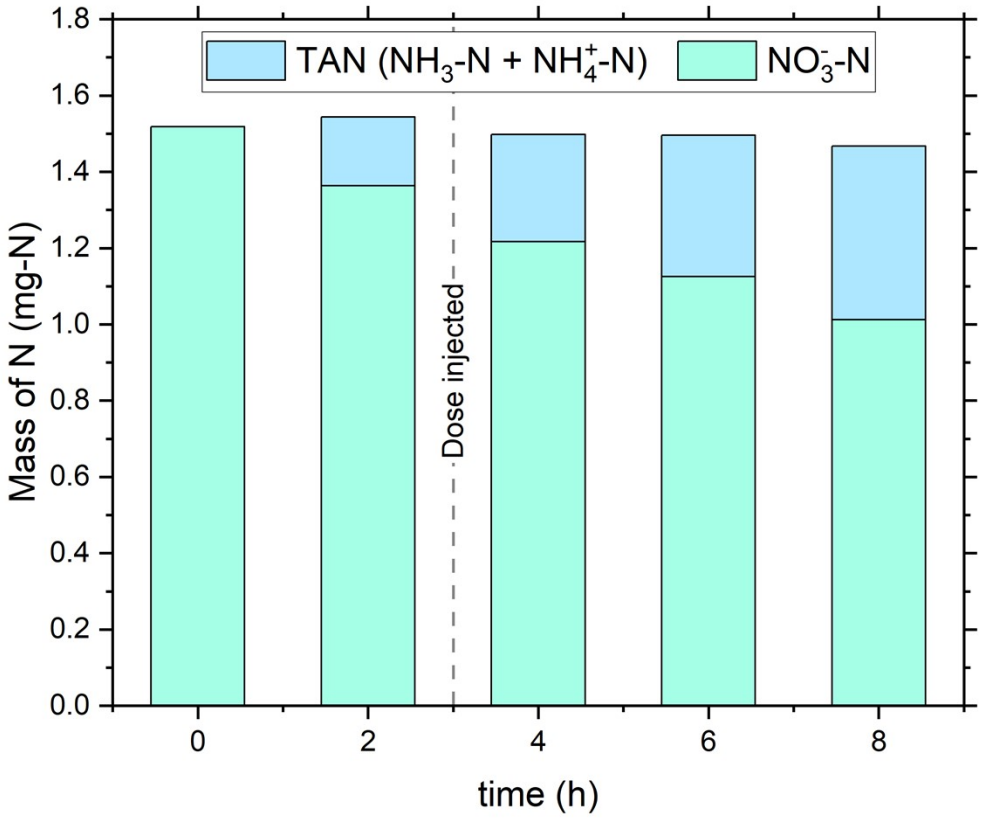

Fig. S17. N mass balance for Ca^{2+} dose two-chamber CPE experiment. 95 µL 1 M $CaCl_2$ injected into the catholyte at t = 2 h.

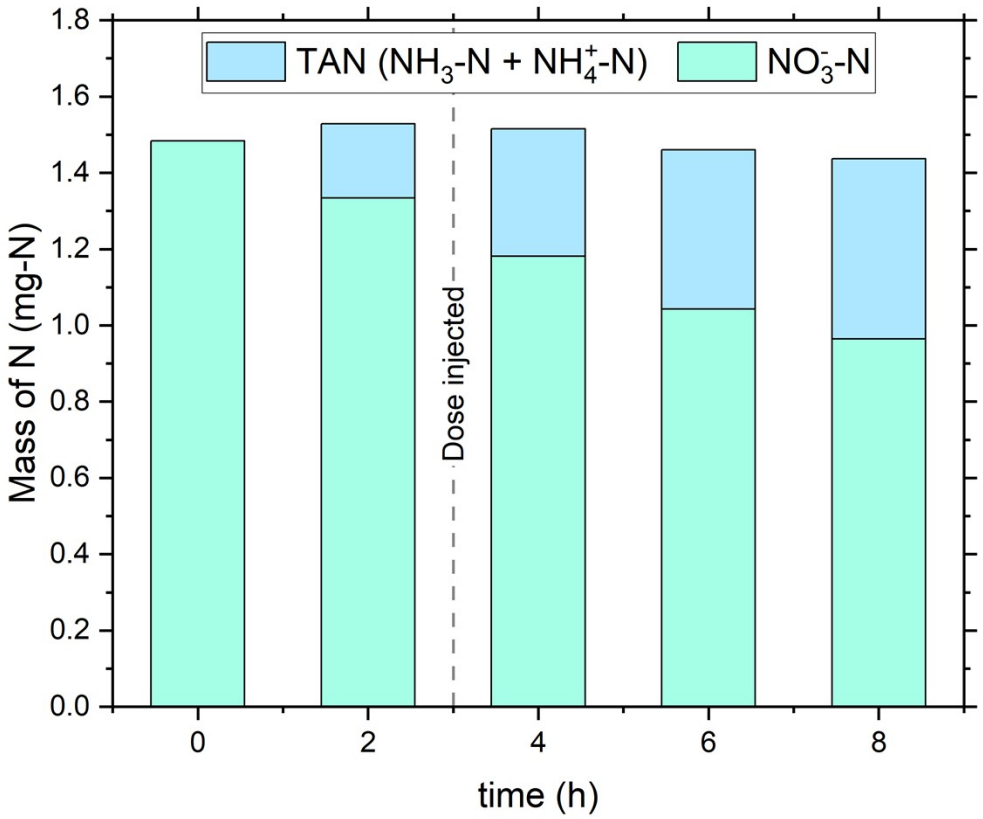

241

242 Fig. S18. N mass balance for Mg^{2+} dose two-chamber CPE experiment. 70 µL 1 M $MgCl_2$ injected into the

243 catholyte at t = 2 h.

244

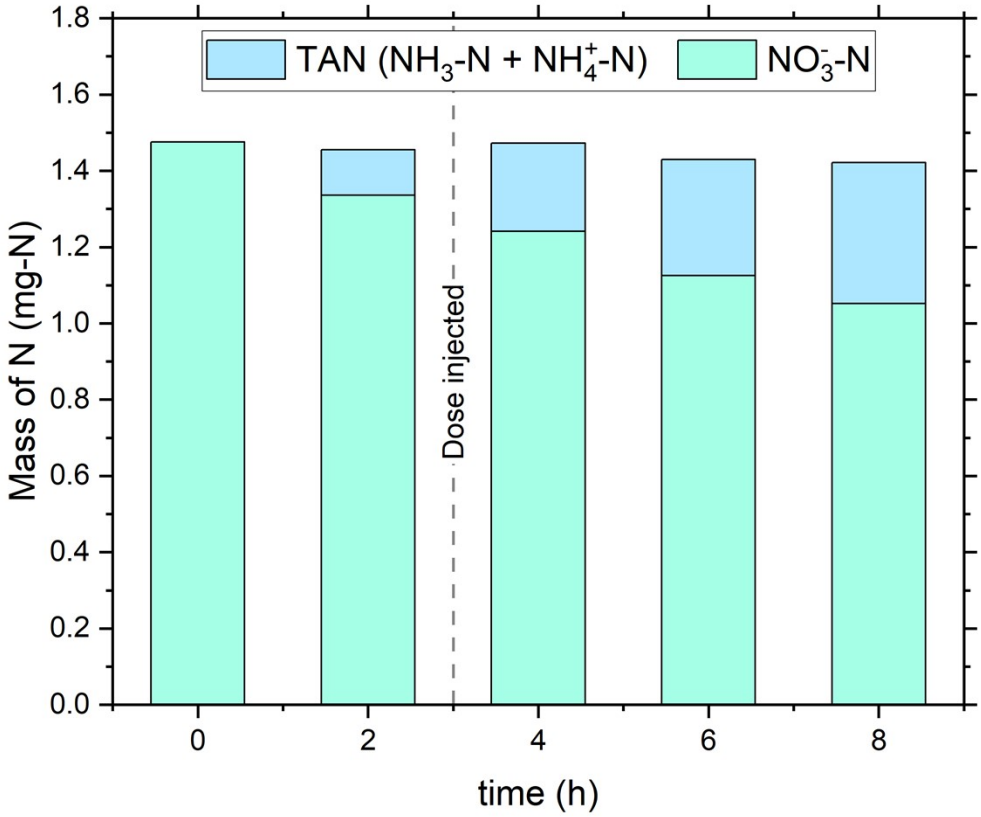

245

246 Fig. S19. N mass balance for $^{HCO_3^-}$ dose two-chamber CPE experiment. 75 µL 1 M $NaHCO_3$ injected into

247 the catholyte at t = 2 h.

248

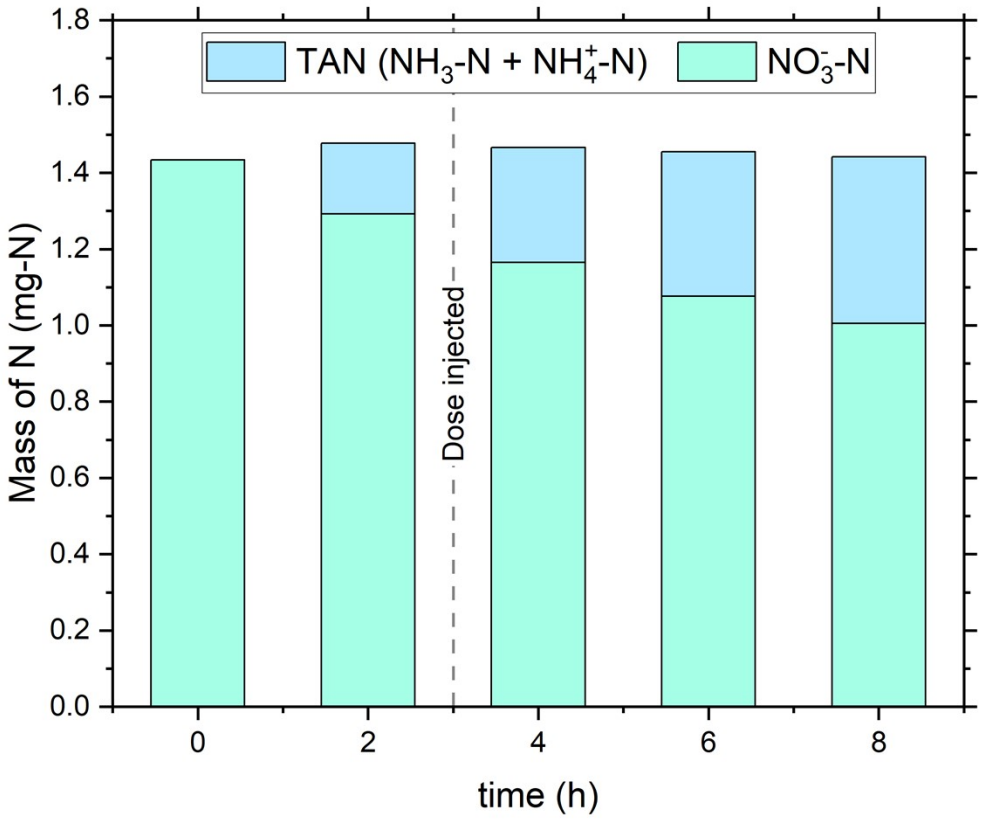

249

250 Fig. S20. N mass balance for simultaneous Mg^{2+} and HCO_3^- dose CPE experiment. 75 µL 1 M $NaHCO_3$

251 and 70 µL 1 M $MgCl_2$ injected into the catholyte at t = 2 h.

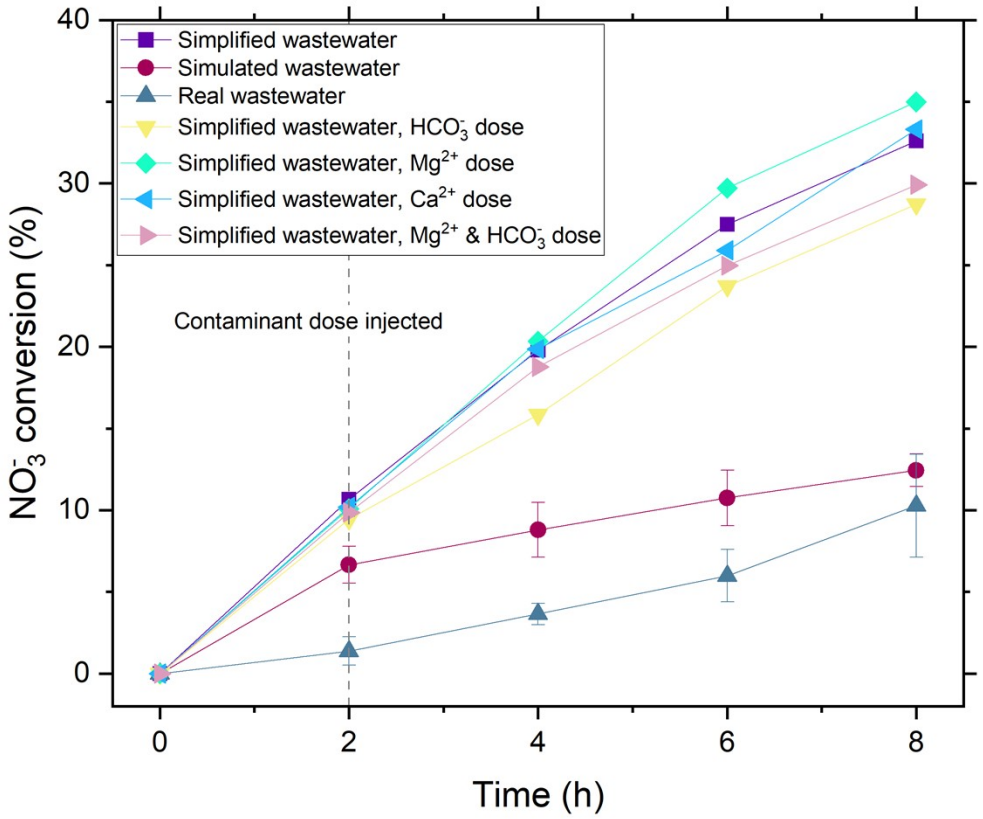

253

254 Fig. S21. Nitrate conversion for contaminant dose two-chamber CPE experiments.

255

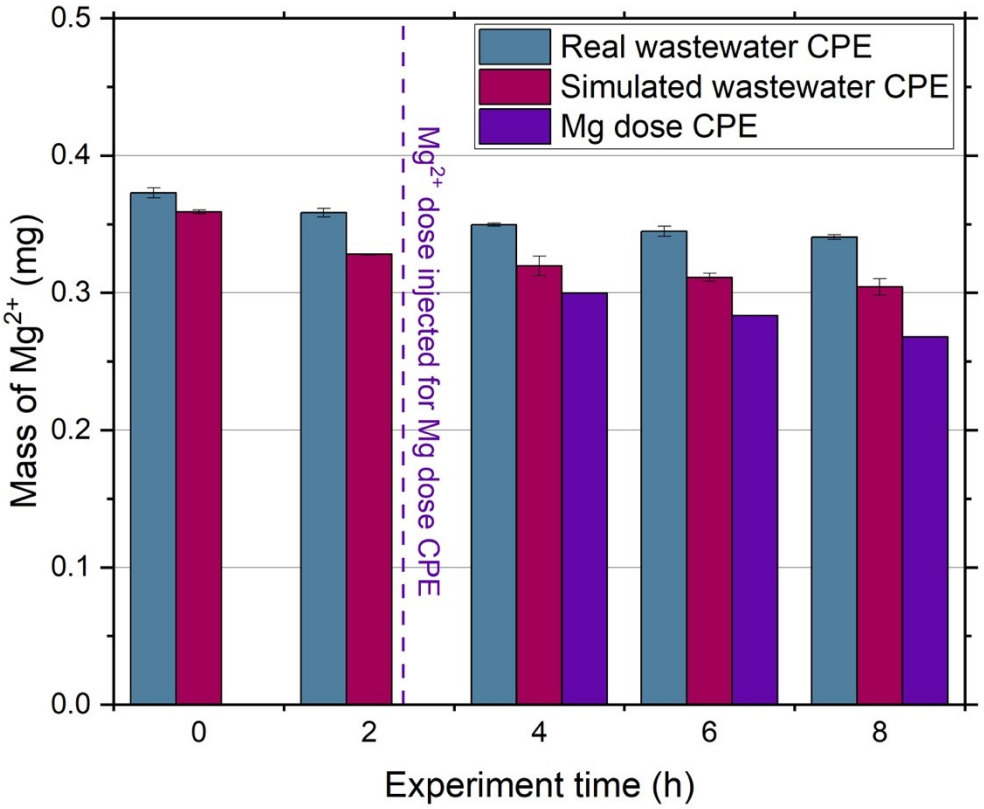

256

257 Fig. S22. Mg mass as a function of time for real wastewater CPE, simulated wastewater CPE, and Mg dose
258 CPE. Error bars represent ± one standard deviation from triplicate experiments (n=3). Note that Mg dose
259 CPE data are from one experiment. Consumption of Mg in real wastewater CPE: 8.6 ± 1.3%. Consumption
260 of Mg in Simulated wastewater CPE: 15.3 ± 1.3%. Consumption of Mg in Mg dose CPE: 10.6%.

261

Section S5: Electrocatalyst-in-a-box (ECaB)

Section S5.1: Equations used to evaluate ECaB

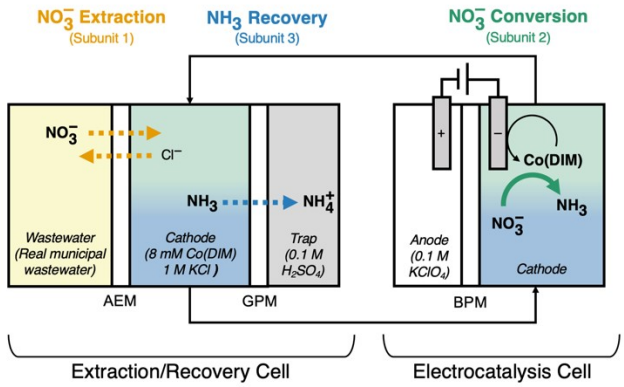

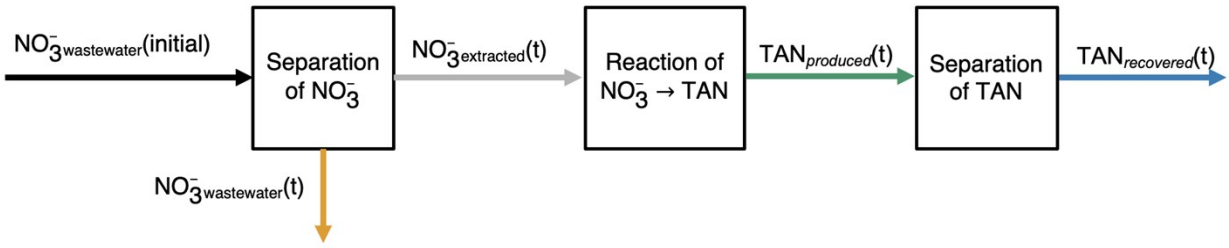

Efficiencies

$$\eta_{NO_3^-,extraction} = \left(\frac{mol\ NO_3^-_{wastewater}(initial) - mol\ NO_3^-_{wastewater}(t)}{mol\ NO_3^-_{wastewater}(initial)}\right) = \left(\frac{mol\ NO_3^-_{extracted}(t)}{mol\ NO_3^-_{wastewater}(initial)}\right) \quad \text{(Equation S5.1.1)}$$

$$X_{NO_3^-}(t) = \frac{mol\ NO_3^-_{extracted}(0\ h\ CPE) - mol\ NO_3^-_{extracted}(t)}{mol\ NO_3^-_{extracted}(t)} = \frac{mol\ NO_3^-_{converted}(t)}{mol\ NO_3^-_{extracted}(t)} \quad \text{(Equation S5.1.2)}$$

$$Y_{TAN} = X_{NO_3^-} * S_{TAN} = \frac{mol\ TAN_{produced}(t)}{mol\ NO_3^-_{extracted}(t)},$$

where for ECaB, $mol\ TAN_{produced}(t) = mol\ TAN_{catholyte}(t) + mol\ TAN_{trap}(t)$ (Equation S5.1.3)

$$\eta_{TAN,recovery} = \left(\frac{mol\ TAN_{trap}(t)}{mol\ TAN_{produced}(t)}\right) = \left(\frac{mol\ TAN_{recovered}(t)}{mol\ TAN_{produced}(t)}\right) \quad \text{(Equation S5.1.4)}$$

$$\eta_{N\ recovery,overall} = \left(\frac{mol\ TAN_{recovered}(t)}{mol\ NO_3^-_{wastewater}(initial)}\right) \quad \text{(Equation S5.1.5)*}$$

$$\eta_{N\ recovery,overall} = \eta_{NO_3^-,extraction} * Y_{TAN} * \eta_{TAN,recovery} = \left(\frac{mol\ TAN_{trap}(t)}{mol\ NO_3^-_{wastewater}(initial)}\right) \quad \text{(Equation S5.1.6)*}$$

274

275 $*\eta_{N\ recovery,overall}$ for ECaB was calculated by Equations S5 and S6 and both datasets are shown in Fig. SX. Data

276 calculated by Equations S5 and S6 are in agreement within experimental error for all time points.

$$FE\ to\ TAN\ (\%) = \left(\frac{n * F *\ mol\ TAN_{produced}}{Q_{passed}}\right) * 100\%$$

277 (Equation S5.1.7)

278 where $n = number\ of\ electrons\ (8)\ required\ to\ produce\ one\ mole\ of\ TAN\ from\ NO_3^-$,

279 $Q_{passed} = charge\ passed\ in\ CPE\ in\ units\ of\ C$, and $F = 96485\ C\ mol^{-1}$

280

281 **Rates**

$$Areal\ NO_3^-\ extraction\ rate = \frac{mol\ NO_{3\ extracted}^-(t)}{t * A_{cross\ sectional}}$$

282 (Equation S5.1.8)

$$Volumetric\ NO_3^-\ extraction\ rate = \frac{mol\ NO_{3\ extracted}^-(t)}{t * V_{wastewater}}$$

283 (Equation S5.1.9)

$$Areal\ NO_3^-\ conversion\ rate = \frac{mol\ NO_{3\ converted}^-(t_{CPE})}{t_{CPE} * A_{cross\ sectional}}$$

284 (Equation S5.1.10)

$$Volumetric\ NO_3^-\ conversion\ rate = \frac{mol\ NO_{3\ converted}^-(t_{CPE})}{t_{CPE} * V_{catholyte}}$$

285 (Equation S5.1.11)

$$Areal\ TAN\ production\ (yield)\ rate = \frac{mol\ TAN_{produced}(t_{CPE})}{t_{CPE} * A_{cross\ sectional}}$$

286 (Equation S5.1.12)

$$Volumetric\ TAN\ production\ (yield)\ rate = \frac{mol\ TAN_{produced}(t_{CPE})}{t_{CPE} * V_{catholyte}}$$

287 (Equation S5.1.13)

$$Areal\ TAN\ recovery\ rate = \frac{mol\ TAN_{recovered}(t)}{t * A_{cross\ sectional}}$$

288 (Equation S5.1.14)

$$Volumetric\ TAN\ recovery\ rate = \frac{mol\ TAN_{recovered}(t)}{t * V_{catholyte}}$$

289 (Equation S5.1.15)

$$Psuedo\ instant.\ \left[NO_3^-\right]\ normalized\ conversion\ rate = \frac{mol\ NO_{3\ converted}^-(t) - mol\ NO_{3\ converted}^-(t-1)}{C_{NO_{3\ catholyte}^-}\ (t-1) * V_{catholyte}}$$

290 (Equation S5.1.16)

291

Energy consumption

$$Energy\ consumed\ for\ NO_3^-\ extraction = \frac{E_{cell,av} * Q_{passed}}{mol\ NO_{3\ extracted}^-(t)} \quad \text{(Equation S5.1.17)}$$

$$Energy\ consumed\ for\ NO_3^-\ conversion = \frac{E_{cell,av} * Q_{passed}}{mol\ NO_{3\ converted}^-(t)} \quad \text{(Equation S5.1.18)}$$

$$Energy\ consumed\ for\ TAN\ production = \frac{E_{cell,av} * Q_{passed}}{mol\ TAN_{produced}(t)} \quad \text{(Equation S5.1.19)}$$

$$Energy\ consumed\ for\ TAN\ recovery = \frac{E_{cell,av} * Q_{passed}}{mol\ TAN_{recovered}(t)} \quad \text{(Equation S5.1.20)}$$

Electricity operational expenditure

$$Recovered\ (NH_4)_2SO_4\ cost = \frac{E_{cell,av} * Q_{passed}}{mol\ TAN_{recovered}(t)} \times \frac{¢3}{kWh} \quad \text{(Equation S5.1.21)}$$

Equation 5.1.21 was used to calculate the cost of producing purified ammonium sulfate when considering electricity as the only operational expenditure at a cost of ¢3 kWh^{-1}.[7]

Section S5.2: Proof-of-concept ECaB pH, rates, efficiencies, and cathode characterization

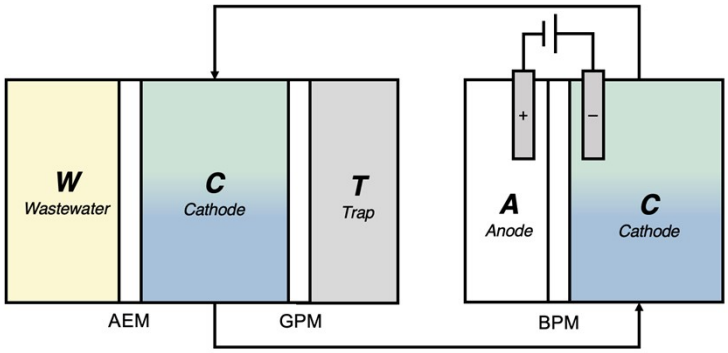

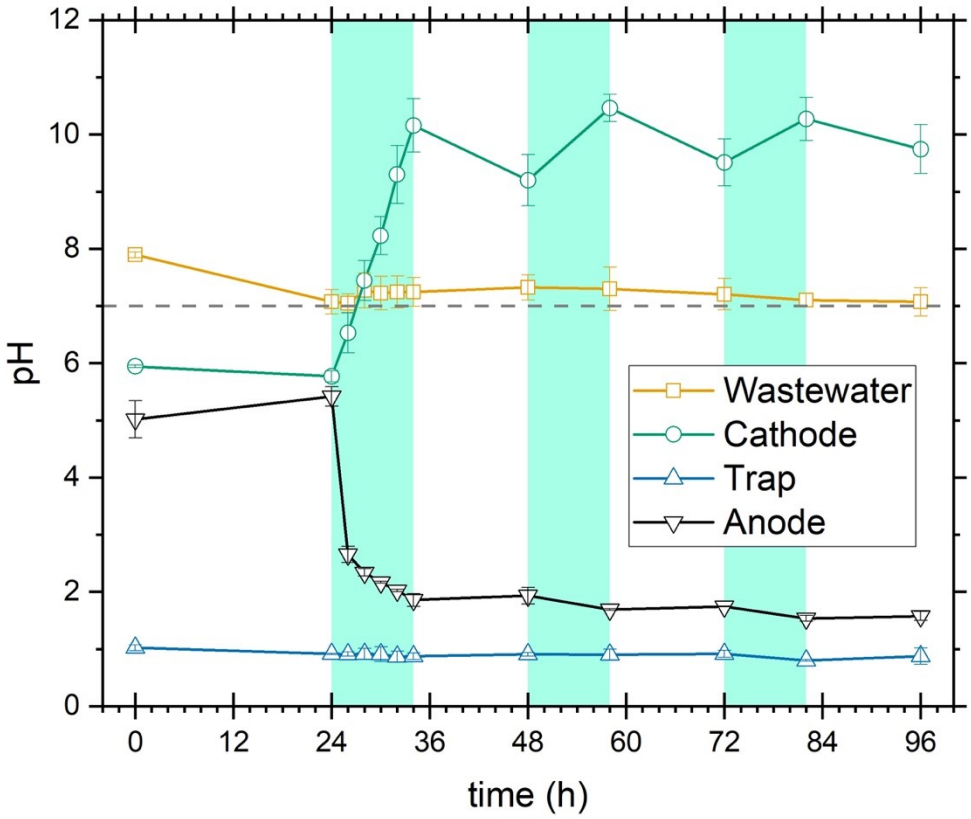

Fig. S23. pH trends of the 4 chambers in proof-of-concept ECaB. Error bars represent ± one standard deviation from triplicate experiments (n=3).

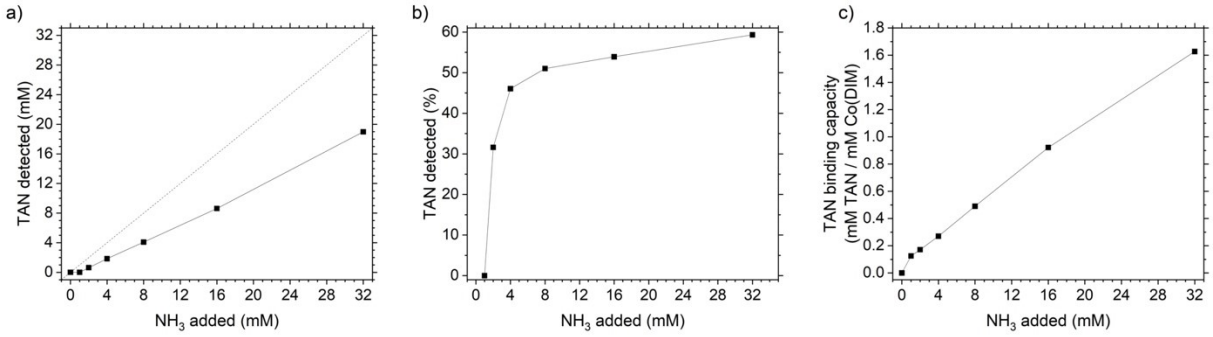

308

309 Fig. S24. Binding of TAN to Co(DIM). Experiments were carried out by adding 0, 1, 2, 4, 8, 16, or 32 mM
310 NH_3 (as NH_4OH) to vials of 1 M KCl + 8 mM Co(DIM), pH 10.5. Vials were shaken vigorously for 4 h,
311 acidified with concentrated H_2SO_4, and then TAN was measured by cation IC. (a) TAN concentration
312 detected by cation IC as a function of NH_3 concentration added. Deviation from the dotted line ($y = x$)
313 indicates TAN adsorption by Co(DIM). (b) Percent of TAN detected as a function of NH_3 added. More of
314 the added nitrogen binds to Co(DIM) at low NH_3 concentrations. (c) Observed TAN binding capacity of
315 Co(DIM).

316

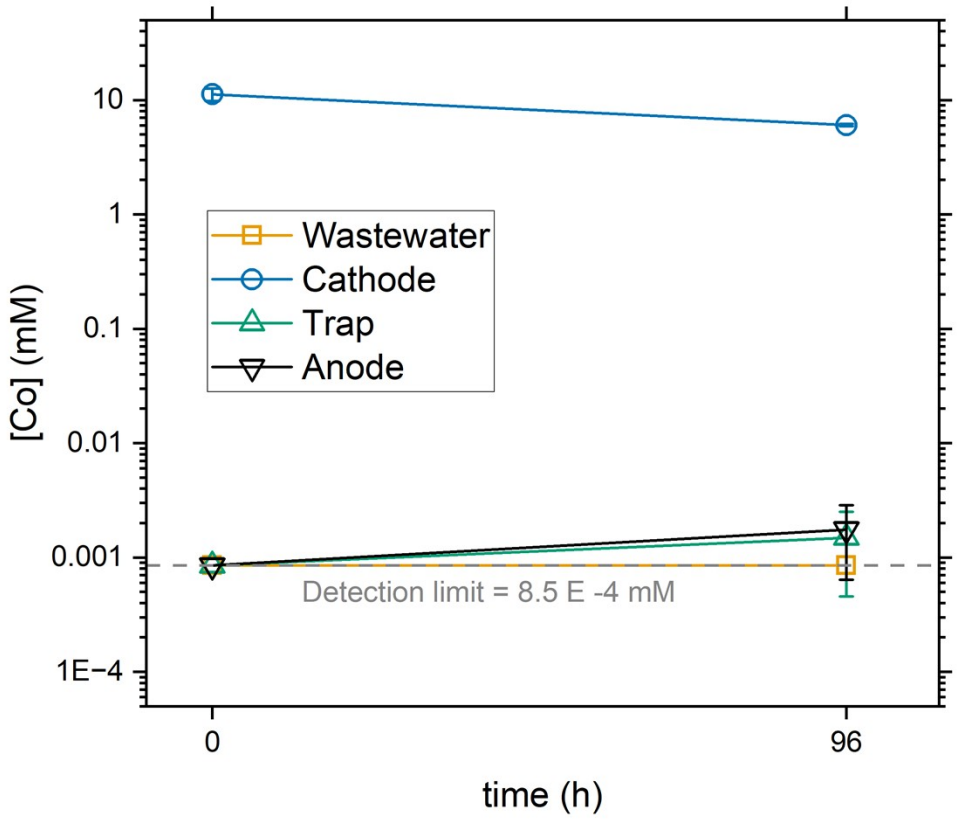

317

318 Fig. S25. Concentration of Co (^{59}Co) in each chamber of proof-of-concept ECaB at initial (0 h) and final
319 (96 h) time points. Co concentration was below detection (0.85 μM) for the initial and final wastewater
320 time points, and for the initial trap and anode time points. These data demonstrate that Co(DIM) remained
321 in the cathode chamber of ECaB proof-of-concept. Error bars represent ± one standard deviation from
322 triplicate experiments (n=3).

323

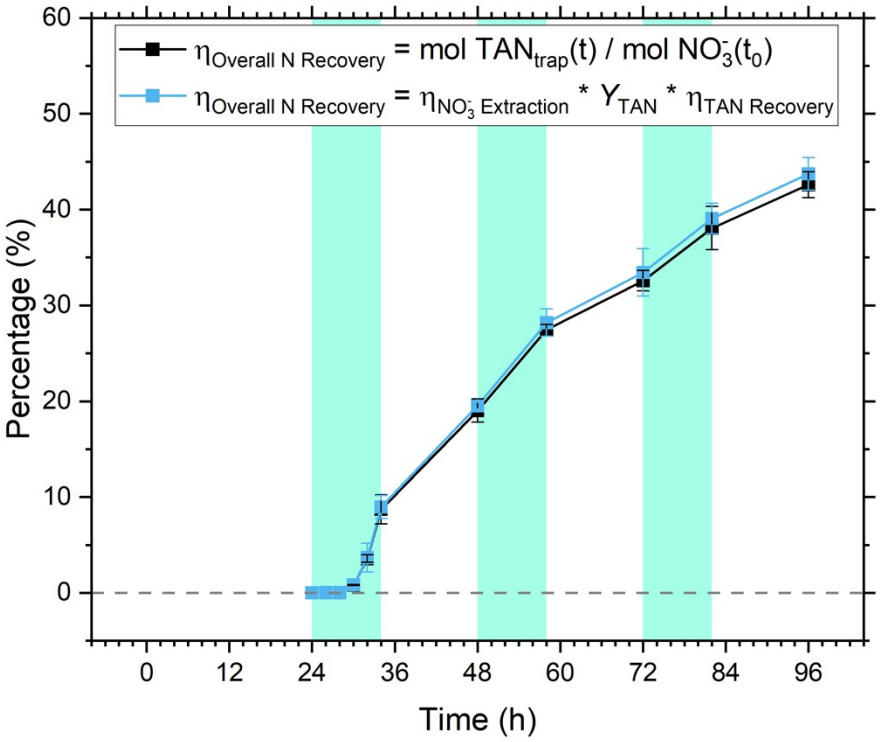

324

325 Fig. S26. Overall N recovery of proof-of-concept ECaB calculated two ways. Black trace was calculated
326 as the mass of TAN in the trap divided by the initial mass of nitrate-nitrogen in the wastewater (Equation
327 S5.1.5). Blue was calculated by multiplying the nitrate extraction efficiency, the yield of TAN, and the
328 TAN recovery efficiency (Equation S5.1.6). Error bars represent ± one standard deviation from triplicate
329 experiments (n=3).

330

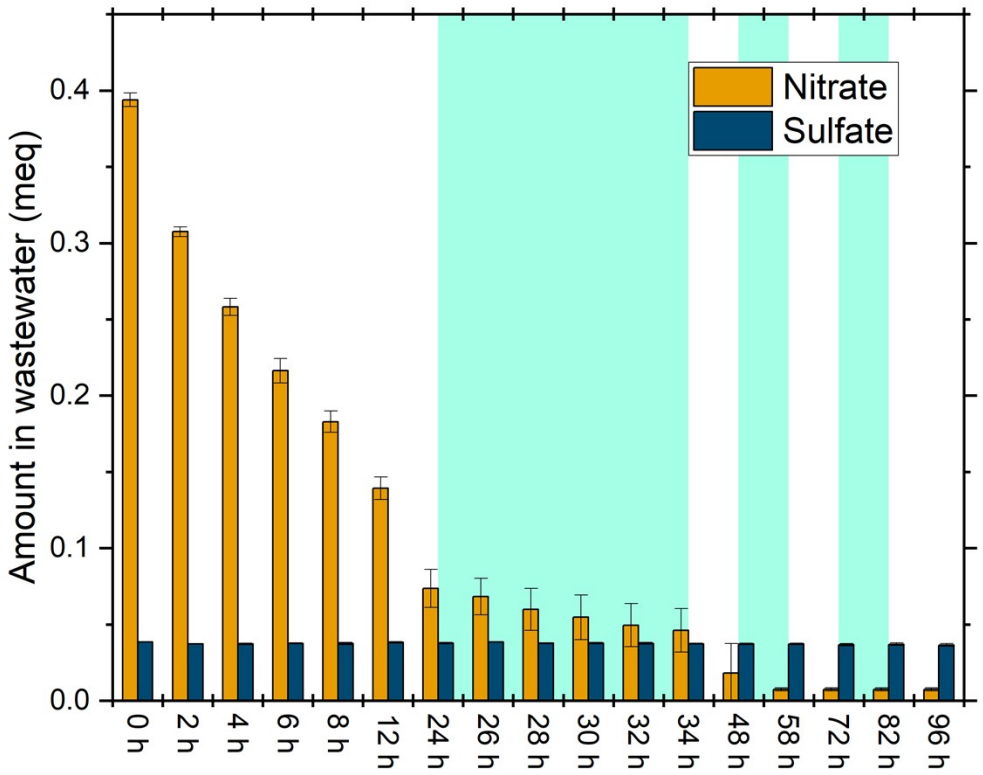

331

332 Fig. S27. Amount (in milliequivalents of charge) of nitrate and sulfate ions in wastewater chamber as a
333 function of time for proof-of-concept ECaB. Error bars represent ± one standard deviation from triplicate
334 experiments (n=3).

335

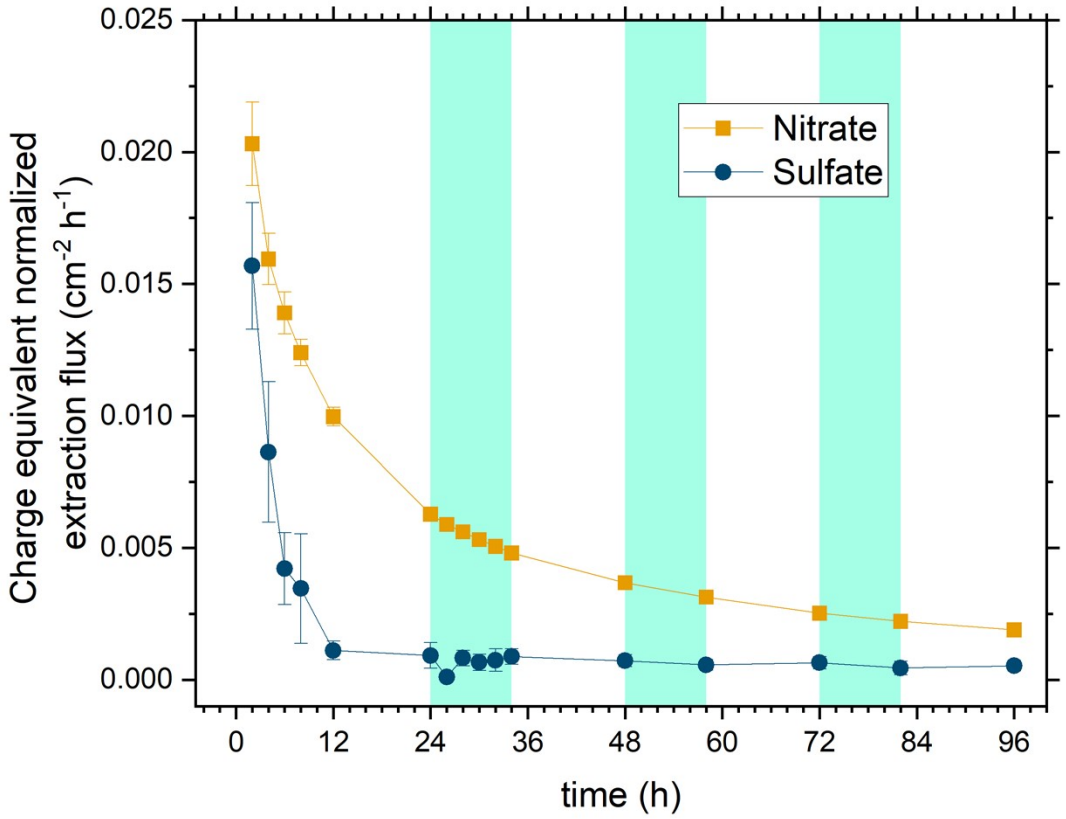

336

337 Fig. S28. Extraction flux (normalized to concentration in milliequivalents of charge) of nitrate and sulfate
338 ions as a function of time for proof-of-concept ECaB. Error bars represent ± one standard deviation from
339 triplicate experiments (n=3).

340

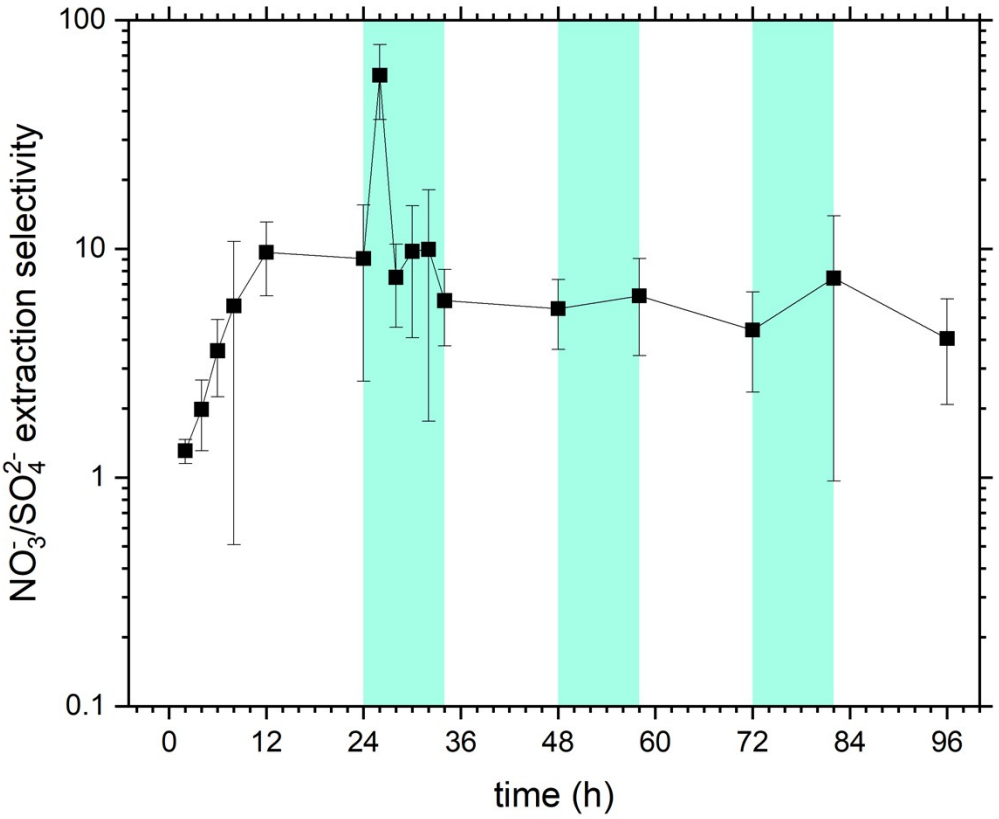

341

342 Fig. S29. Extraction selectivity (calculated as the fraction of nitrate flux divided by sulfate flux) of nitrate
343 ions over sulfate ions as a function of time for proof-of-concept ECaB. Error bars represent ± one standard
344 deviation from triplicate experiments (n=3).

345

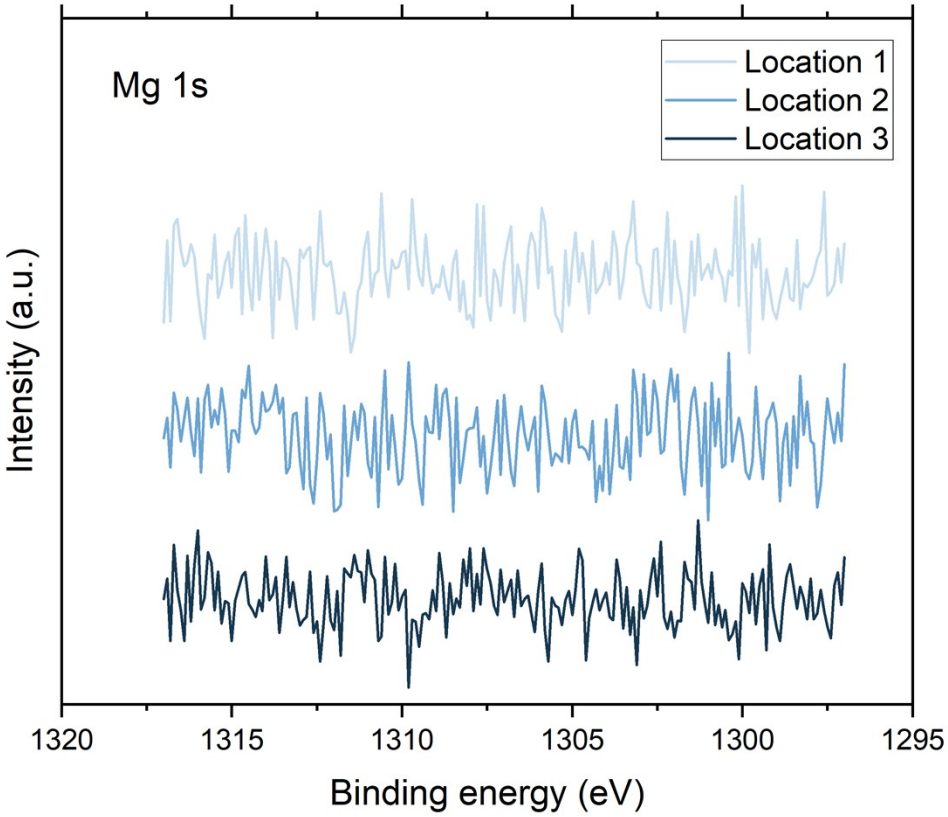

346

347 Fig. S30. XPS Mg 1s scans at three locations of one glassy carbon cathode after proof-of-concept ECaB

348 experiment.

349

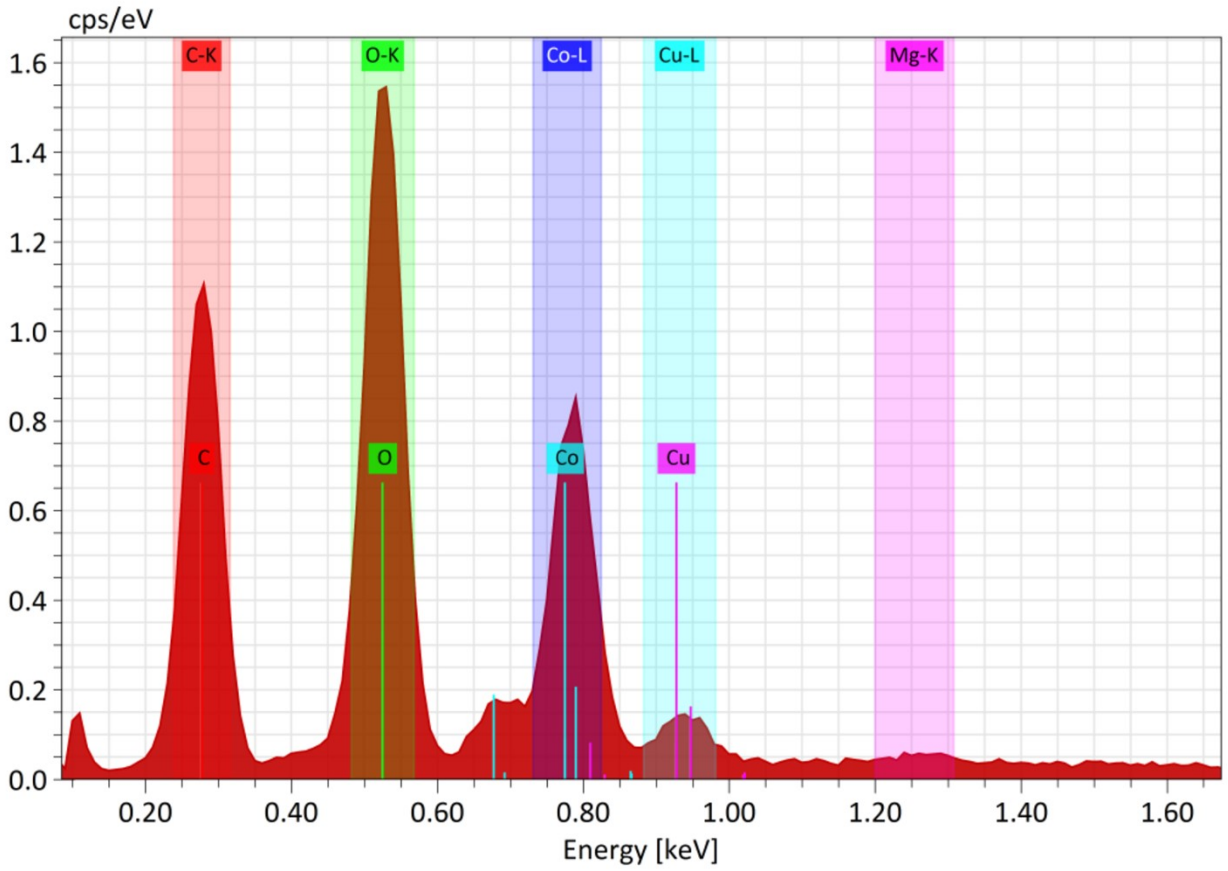

Fig. S31. EDS spectrum of glassy carbon cathode after proof-of-concept ECaB experiment. A small amount of Cu was found on the surface, presumably the from Cu tape used as electrical leads to the GC plate cathode and mixed-metal oxide anode.

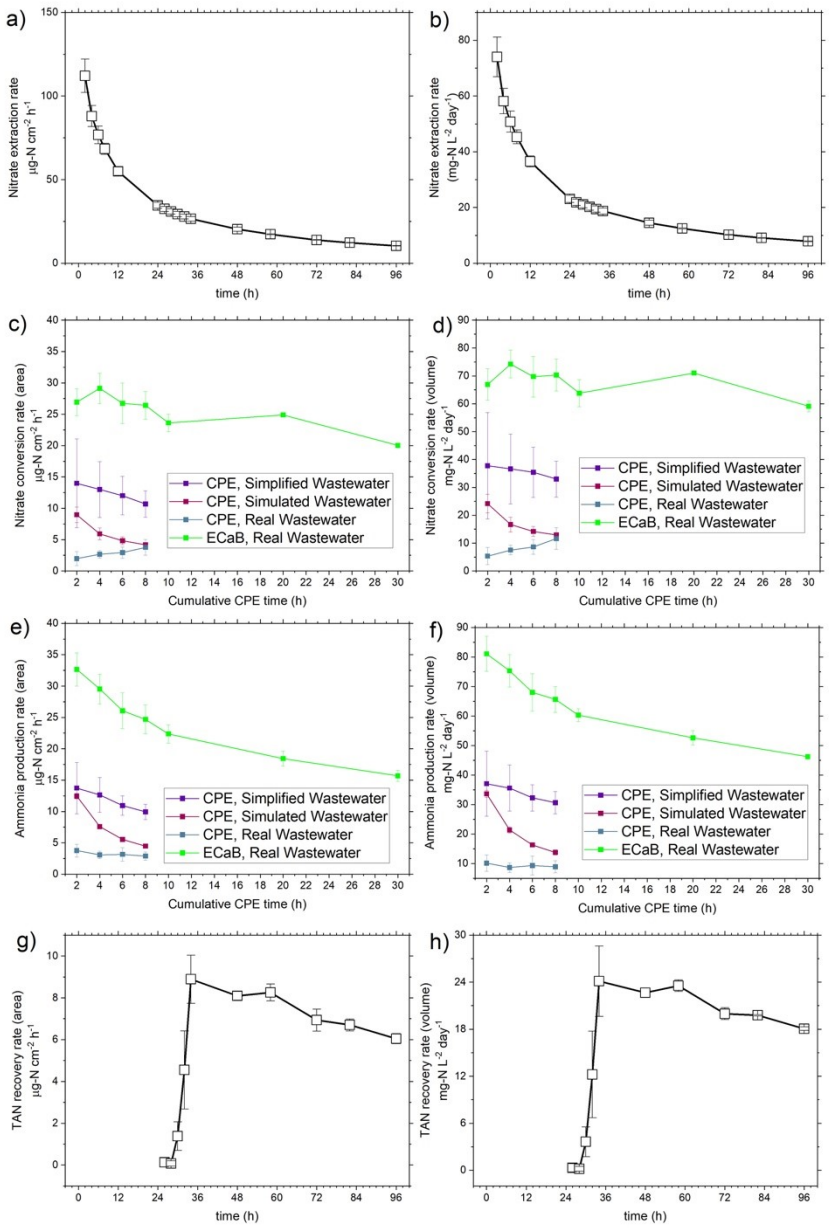

355

356 Fig. S32. a) Areal (normalized to AEM area) and b) volumetric (normalized to wastewater volume) nitrate
357 extraction rates. c) Areal (normalized to GC area) and d) volumetric (normalized to catholyte volume)
358 nitrate conversion rates. e) Areal (normalized to GC area) and f) volumetric (normalized to catholyte
359 volume) TAN yield rates. For nitrate conversion and TAN yield time is cumulative time of CPE. g) Areal
360 (normalized to GPM area) and h) volumetric (normalized to catholyte volume) TAN recovery rates. AEM,
361 GC, and GPM had the same geometric surface area (5.4 cm2). Error bars represent ± one standard deviation
362 from triplicate experiments (n=3) of proof-of-concept ECaB.

Section S6: Donnan dialysis equilibrium calculations

In Donnan dialysis, an ion exchange membrane separates a wastewater (or feed solution) and a saline electrolyte (or receiving solution). Ion exchange between the two solutions is driven by an electrochemical potential gradient for each ion *i* in the system. More concretely, Donnan dialysis was employed in this work using a concentrated Cl^- electrolyte as the receiving solution and NO_3^--rich municipal secondary effluent as the feed solution. When separated by an AEM, feed NO_3^- ions spontaneously exchange with receiver Cl^- ions in the synthetic electrolyte, while cation migration is precluded by the fixed positive charges in the membrane.

Section S6.1: System of equations (ion mass balances, electroneutrality, and Donnan equilibrium)

In this section, we provide a system of equations used to model equilibrium conditions for a Donnan dialysis (DD) process. We show general equations which can be applied to any number of ions *i* in a system where there is a feed solution (FS) and receiving solution (RS) separation by an ion exchange membrane. For the DD process in this work, we consider only Cl^- and NO_3^- because the monovalent-selective anion exchange membrane (AEM) used in ECaB experiments was selective against SO_4^{2-} migration and rejected cation migration. Fig. S31 shows predicted equilibrium conditions for DD as a function of feed to receiving solution volume ratios.

1. Mass balance

$$C_{i,FS,0}V_{FS} + C_{i,RS,0}V_{RS} = C_{i,FS,equil.}V_{FS} + C_{i,RS,equil.}V_{RS} \quad \text{(Equation S6.1.1)}$$

2. Electroneutrality

$$\sum_i z_i(C_{i,FS,0}V_{FS}) = \sum_i z_i(C_{i,FS,equil.}V_{FS}) \quad \text{(Equation}$$

$$\sum_i z_i(C_{i,RS,0}V_{RS}) = \sum_i z_i(C_{i,RS,equil.}V_{RS}) \quad \text{(Equation S6.1.3)}$$

386

387 3. Solution phase electrochemical potential equations for Donnan equilibrium

388 $$\bar{\mu}_{i,FS,\,equil.} = \bar{\mu}_{i,RS,\,equil.} \quad \text{(Equation S6.1.4)}$$

389 $$\mu_i^0 + RT\,ln a_{i,\,FS,equil.} + z_i F\psi_{FS,\,equil.} = \mu_i^0 + RT\,ln a_{i,\,RS,equil.} + z_i F\psi_{RS,\,equil.} \quad \text{(Equation S6.1.5)}$$

390 Rearranging Equation S6.1.5 yields an equality between the electrochemical potential difference

391 arising from the activity of each ion *i* in feed and receiving streams, and the electrochemical potential

392 difference arising from the electric potential difference across the membrane.

393 $$z_i F\psi_{FS,\,equil.} - z_i F\psi_{RS,\,equil.} = RT\,ln a_{i,\,RS,equil.} - RT\,ln a_{i,\,FS,equil.} \quad \text{(Equation S6.1.6)}$$

394 Rearranging Equation S6.1.6 yields an equality between the electric potential difference across the ion

395 exchange membrane and the solution phase electrochemical potential difference.

396 $$\psi_{FS,\,equil.} - \psi_{RS,\,equil.} = \frac{RT}{z_i F} ln\left(\frac{a_{i,\,RS,equil.}}{a_{i,\,FS,equil.}}\right) \quad \text{(Equation S6.1.7)}$$

397 Making the approximation that the electric potential difference experienced by each ion *i* in the system is

398 the same, the right hand side of Equation S6.1.7 can be used to equate electrochemical potentials of dissimilar ions.

399 For our example, the electrochemical potentials of Cl^- and NO_3^- can be equated as in Equations S6.1.8 and S6.1.9.

400 $$\frac{RT}{-1 * F} ln\left(\frac{a_{Cl^-,\,RS,equil.}}{a_{Cl^-,\,FS,equil.}}\right) = \frac{RT}{-1 * F} ln\left(\frac{a_{NO_3^-,\,RS,equil.}}{a_{NO_3^-,\,FS,equil.}}\right) \quad \text{(Equation S6.1.8)}$$

401 $$ln\left(\frac{a_{Cl^-,\,RS,equil.}}{a_{Cl^-,\,FS,equil.}}\right) = ln\left(\frac{a_{NO_3^-,\,RS,equil.}}{a_{NO_3^-,\,FS,equil.}}\right) \quad \text{(Equation S6.1.9)}$$

402 The activities used in Donnan equilibrium equations were considered for both and ideal model and a Pitzer

403 model based on the concentration of ions in the catholyte.[8–11]

404 For ideal model: $a_i = C_i[M]$ (Equation S6.1.10)

405 For Pitzer model: $a_i = \gamma_i C_i[M]$ (Equation S6.1.11)

406

407

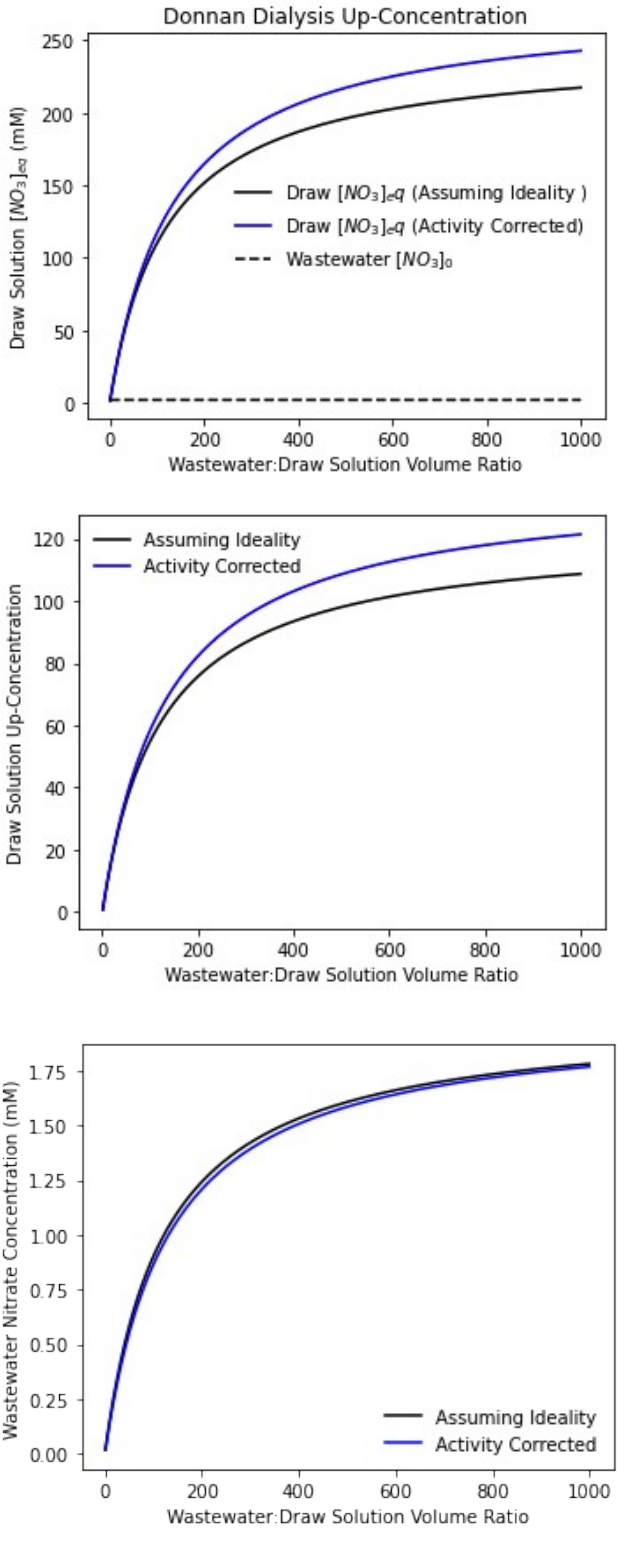

408

409

410 Fig. S33. Equilibrium conditions for Donnan dialysis with secondary effluent wastewater feed and 1 M KCl

411 receiving solution.

Section S7: ECaB process engineering and targets

Section S7.1: Subunit engineered ECaB performance

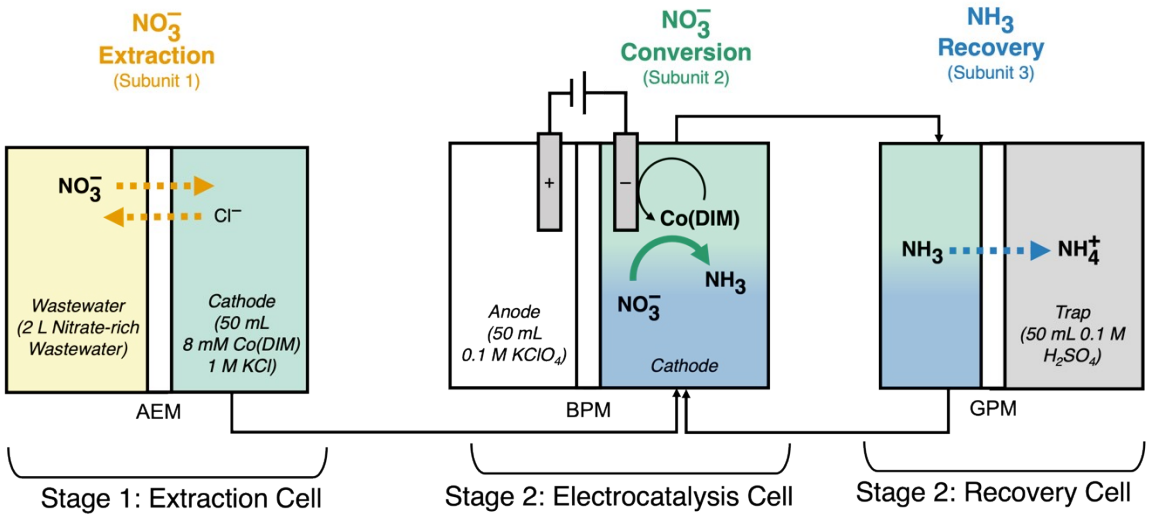

Fig. S34. Subunit engineered ECaB configuration used to demonstrate improved extraction and converstion rates. To improve extraction from proof-of-concept, we used 2 L (increased from 200 mL) of wastewater (to increase up-concentration) and a commercial serpentine flow field electrolyzer (to reduce mass transport limitations). The resulting catholyte was used in the same commercial electrolyzer to perform Co(DIM)-mediated NO_3RR. TAN recovery was performed in parallel with nitrate conversion using the same experimental setup as in proof-of-concept.

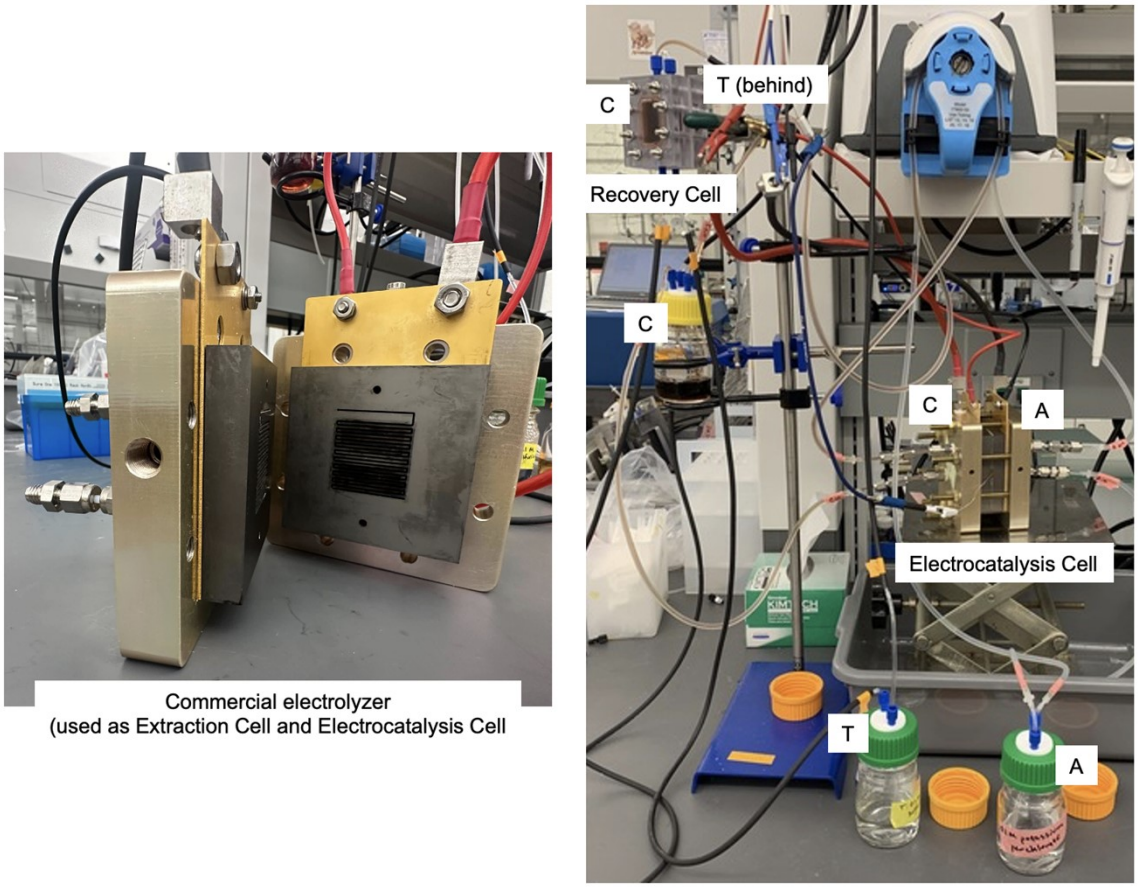

422

423 Fig. S35. Photos of the commercial electrolyzer (left) and the electrocatalysis cell and recovery cell in

424 operation (right). Catholyte (C), anolyte (A), and trap (T) chambers and recirculation bottles are labeled.

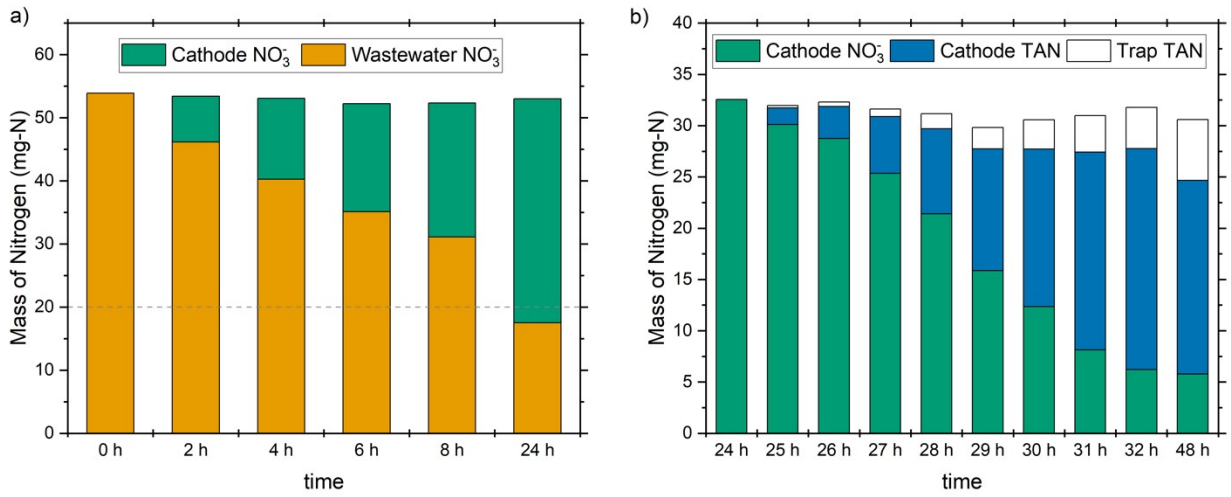

425

426 Fig. S36. Nitrogen mass balance for subunit engineered ECaB (a) Donnan dialysis nitrate extraction and
427 (b) Co(DIM)-mediated NO_3RR (nitrate conversion and TAN production) of the resulting catholyte. The
428 dashed horizontal line in panel (a) describes the mass of nitrogen that must be removed from the wastewater
429 to achieve an effluent concentration of 10 mg-N/L; subunit engineered ECaB was able to achieve this
430 concentration in 24 h with 2 L of wastewater feed. 67.5% of nitrate was extracted in 24 h, and 80.8% of the
431 extracted nitrate was converted to TAN in 8 h of CPE.

432

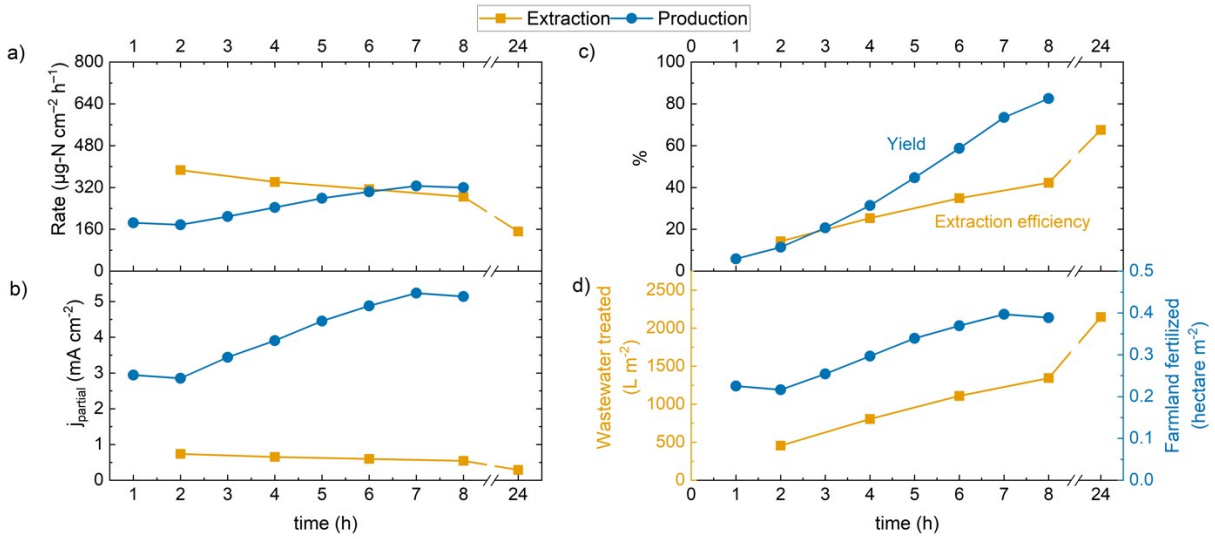

433

434 Fig. S37. Rates of nitrate extraction (orange) and TAN production (green) expressed as (a) flux of nitrogen
435 and (b) partial current density. In Panel (b), extraction partial current density is an effective ionic current
436 density of nitrate crossing the AEM from wastewater to catholyte (balanced by an equal and opposite flux
437 of chloride crossing the AEM from catholyte to wastewater); no external current was applied during
438 extraction. (c) Nitrate extraction efficiency and TAN yield. (d) Area-normalized volume of wastewater
439 treated and farmland serviced with $(NH_4)_2SO_4$ fertilizer. Farmland serviced was calculated by assuming a
440 rate of 72 kg-N hectare^{-1} year^{-1}: the average fertilizer application rate of crops in the United States.[12]

441

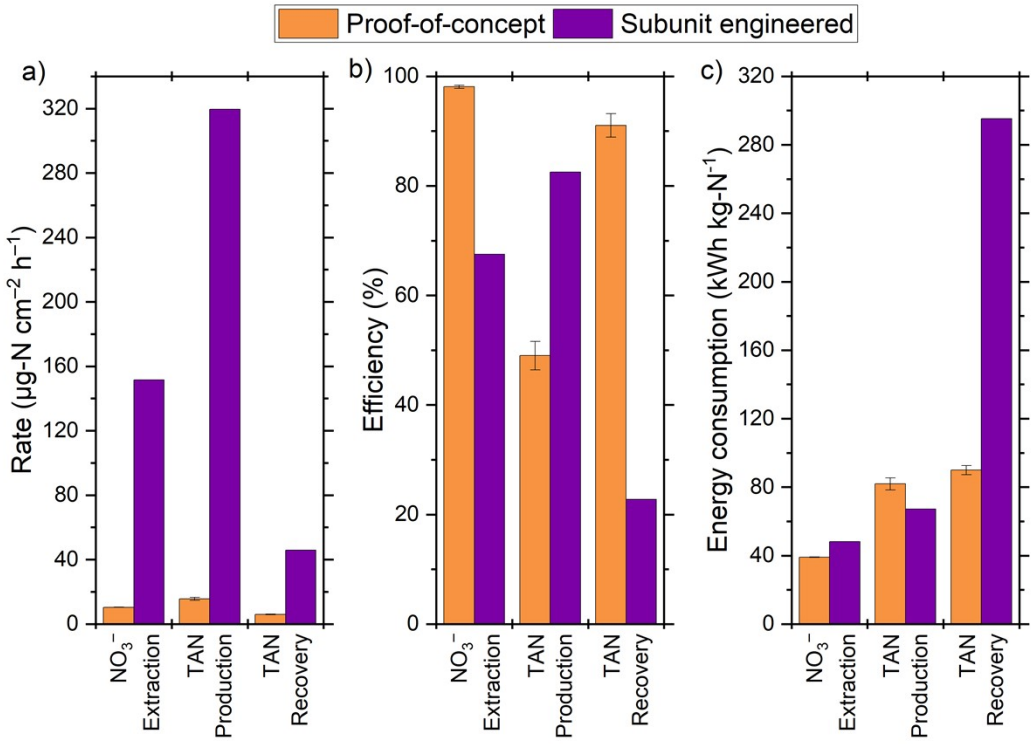

442

443 Fig. S38. (a) Rates, (b) efficiencies, and (c) energy consumption of nitrate extraction, TAN production, and
444 TAN recovery in proof-of-concept ECaB (orange) and subunit engineered ECaB (purple). These data are
445 the same that appear in Extended Data Tables 1, 3, and 4. Error bars represent ± one standard deviation
446 from triplicate experiments (n=3) for proof-of-concept ECaB. Data points for subunit engineered ECaB do
447 not have error bars because only one experiment was performed.

448

Section S7.2: Simplified cost assessment

Our cost assessment used the flux of NO_3^- from a municipal wastewater treatment plant processing $10^7\ gal_{\text{wastewater}}\ \text{day}^{-1}$ (the size of a large municipal wastewater treatment facility)[13] with 28 mg-NO_3-N L^{-1} as the basis for electricity consumption (a total NO_3RR current to convert all nitrate to TAN), chemical inputs (NaCl for nitrate extraction and H_2SO_4 for TAN recovery), and revenue ($(NH_4)_2SO_4$ fertilizer sales). NO_3RR overpotential (η_{NO3RR}) was calculated using the standard reduction potential of NO_3RR to ammonia (+0.7 V_{RHE})[14] and the Nernst equation assuming a steady state pH of 10 to facilitate TAN recovery by membrane stripping. Total charge required was calculated assuming a removal efficiency of 64.2% such that the effluent concentration was 10 mg-NO_3-N L^{-1}. OER overpotential (η_{OER}) was calculated using the standard reduction potential of OER (+1.23 V_{RHE}) and the Nernst equation assuming a steady state pH of 1.5 observed in subunit engineered ECaB experiment. Based on the FE_{TAN}, η_{NO3RR}, and η_{OER}, the required energy consumption was calculated. Multiplying this value by the electricity cost yielded the operational expenditure (OpEx) for electricity. We also calculated the electricity costs associated with pumping according to Tarpeh et al.[15]

$$Pumping\ energy = \frac{1}{mol\ TAN_{produced}}\left(\frac{t\gamma V H^*}{n^*_{pump} n^*_{motor}}\right) \quad \text{Equation S7.2.1}$$

In equation S7.2.1, t is the duration of pumping wastewater through the extraction cell (24 hours), γ is the specific weight of water (9.8 kN m^{-3}), V is the flow rate (57 mL min^{-1}), H^* is the pump head determined by the length of the serpentine flow path in the extraction cell required to treat $10^7\ gal_{\text{wastewater}}\ \text{day}^{-1}$ (1.2×10^7 m), n^*_{pump} is the pump efficiency (assumed 0.4), and n^*_{motor} is the motor efficiency (assumed 0.95). We subtracted this electricity OpEx value and chemical inputs OpEx value from the revenue of recovered $(NH_4)_2SO_4$ fertilizer ($2.77 kg-$N^{-1}$) to establish a yearly cash flow.[16] To correct for inflation, the yearly cash flow was modified by Equation S7.2.2:

$$Cash\ flow(year\ i) = (Revenue(year\ i) - Electricity\ costs(year\ i) - Chemical\ costs(year\ i) - \dots CapEx(year\ i)) \times 1.03^{i}$$ Equation

The capital expenditure (CapEx) budget was calculated as the net present value of the cash flow over a ten year reactor lifetime with a discount rate of 10%. The entire CapEx budget was spent (i.e., the unit process is a net zero cost) to establish a total surface area of reactor components (Fig. 6a). Dividing the CapEx budget by the sum of the area-normalized prices of Co(DIM), anode material, and cell hardware (graphite for flow field blocks) yielded a total reactor geometric surface area. Dividing the product of total current and FE_{TAN} by the total reactor geometric surface area yielded a TAN partial current density target.

We did not consider the costs of labor, the revenue from water recovery, nor potential regulatory fines from environmental nitrate discharge. Additionally, a cost of electricity above ¢4.08 kWh^{-1} forced the process to be a net cost. For this reason, we considered ¢3 kWh^{-1}, motivated by the U.S. Department of Energy's 2030 SunShot target.[7] Table S3 outlines parameters used for the cost assessment.

Table S3. OpEx and CapEx used in simplified cost assessment of ECaB.

Expenditure	Parameter	Value	Source
OpEx – NO_3RR electricity	Electricity cost	¢3 kWh^{-1}	[7]
OpEx – Chemical inputs	Sodium chloride (NaCl)	¢6.67 kg^{-1}	[17]
	Sulfuric acid (H_2SO_4)	¢7.6 kg^{-1}	[17]
OpEx – Pumping electricity	Electricity cost	¢3 kWh^{-1}	[15]
CapEx – Co(DIM)	Cobalt acetate	¢23.7 g^{-1}	Sigma
	1,2-bis(3-aminopropylamino)ethane	¢40.4 mL^{-1}	
	Biacetyl	¢33.6 mL^{-1}	
	Methanol	\$11.90 L^{-1}	
	Perchloric acid (70 wt%)	¢15.6 mL^{-1}	
	Hydrobromic acid (48 wt%)	¢12.9 mL^{-1}	
	Total cost	\$3.97 $g_{Co(DIM)}^{-1}$ (¢8.6 cm^{-2})	
CapEx – Anode	Platinized titanium mesh	\$1.25 cm^{-2}	Fuel Cell

			Store
	Nickel foil	¢7.85 cm^{-2}	McMaster
CapEx – Membranes	Anion exchange membrane (AEM)	¢4.43 cm^{-2} (0.16 $cm_{AEM}^{2} cm_{flow\ path}^{-1}$)	Selemion
	Cation exchange membrane (CEM)	¢2.95 cm^{-2}	Selemion
	Gas-permeable membrane (GPM)	¢0.54 cm^{-2}	Parker-Hannifin
CapEx – Cell hardware	Graphite material	¢1.8 cm^{-3} (5.14 $cm_{graphite}^{3} cm_{flow\ field}^{-2}$)	link link

488

Section S7.3: ECaB for nitrite reduction (NO_2RR)

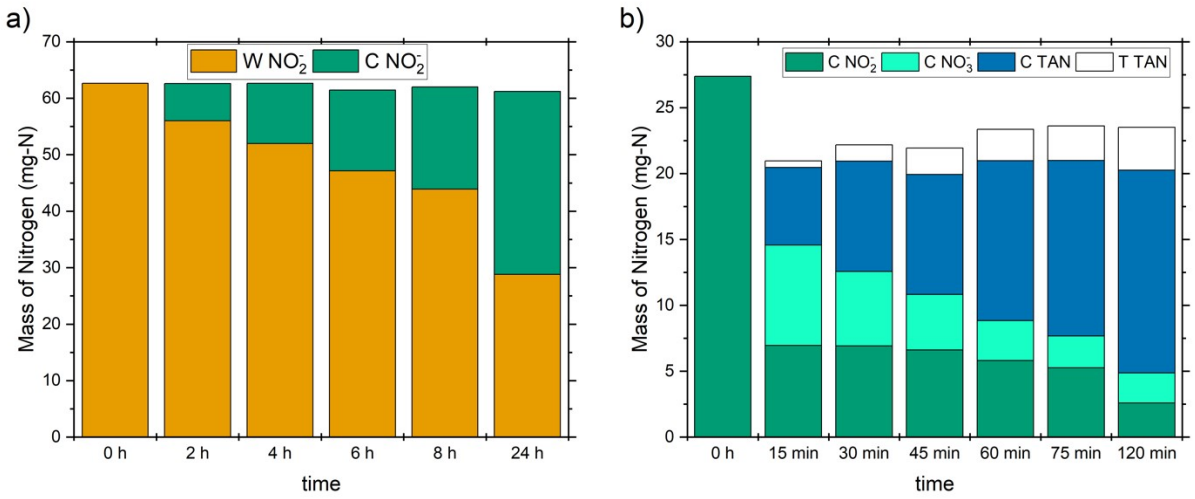

Fig. S39. Nitrogen mass balance for ECaB with Co(DIM)-mediated NO_2RR. (a) Nitrogen mass balance for Donnan dialysis extraction with 2 L of simulated nitrite-bearing wastewater (W; 6.2 mM NaCl, 2 mM $NaNO_2$) and 50 mL of catholyte (C; 1 M KCl, 8 mM Co(DIM). The extraction cell configuration and operation were the same as for subunit engineered ECaB with real wastewater. (b) Nitrogen mass balance for Co(DIM)-mediated nitrite conversion to TAN with concurrent TAN recovery. The conversion cell and trap cell configuration and operation were the same as for the subunit engineered ECaB with real wastewater, except that the constant potential –1.05 V vs. Ag/AgCl was applied for 15 minute increments instead of 1 h increments because Co(DIM)-mediated NO_2RR is significantly faster than Co(DIM)-mediated NO_3RR.

Table S4. Efficiency, rate, and energy comparison to literature: Nitrate extraction

ref	Wastewater	Extraction mechanism	Nitrate extraction efficiency ($\eta_{NO_3^- Extraction}$)	Nitrate extraction rate		Nitrate extraction energy consumption
				$\mu g\ N\ cm^{-2} h^{-1}$	$mg\ N\ L^{-1} day^{-1}$	kWh kg-N^{-1}
*This work	Secondary effluent (2 mM nitrate)	Donnan dialysis (1 M KCl receiver solution)	81.3 ± 3.3% at 24 h 98.1 ± 0.3% at 96 h	34.6 ± 1.7 at 24 h 10.4 ± 0.1 at 96 h	23.0 ± 1.3 at 24 h 7.8 ± 0.1 at 96 h	0 (39.0 ± 0.2 considering all subunits)
*This work	Secondary effluent (2 mM nitrate)	Donnan dialysis (1 M KCl receiver solution)	67.5% at 24 h	151.6 at 24 h	18.2 at 24 h	0 (48.2 considering all subunits)
[18]	Secondary effluent (2 mM nitrate)	n/a				
[19]	Agricultural tile drainage (0.27 mM nitrate)	Electrodeionization with Polyaniline-Co_3O_4-carbon nanotube slurry coated on Ti mesh as electrode	n.r.	n.r.	n.r.	92.2
[20]	25 mM $NaNO_3$ in 0.1 M Na_2SO_4	n/a				
	Printing wastewater (14.9 mM nitrate)	n/a				
[21]	*25 mM $NaNO_3$ in 0.5 M Na_2SO_4*	n/a				
	Pharmaceutical industry wastewater (31.1 ± 1.1 mM nitrate)	n/a				
[22]	Oil refining & chemical catalyst manufacturing wastewater (36.1 ± 0.9 mM nitrate)	n/a				
[23]	*7.14 mM KNO_3*	Electrodialysis, 5 cm^2 (2 M KNO_3 receiver solution)	75.0%	542.4	n.r.	n.r.

*Equations used to calculate ECaB performance metrics in this work are provided in Section S.5.1.

504 Table S5. Efficiency, rate, and energy comparison to literature: Nitrate conversion by NO_3RR

ref	Wastewater	Electrode/catalyst (Geometric surface areas)	Nitrate conversion ($\chi_{NO_3^- Conversion}$)	FE to TAN	Nitrate conversion rate		Nitrate conversion energy consumption
					$\mu g\ N\ cm_{geometric}^{-2} h^{-1}$	$mg\ N\ L^{-1} day^{-1}$	kWh kg-N^{-1}
*This work	Secondary effluent (2 mM nitrate concentrated to 5.8 mM)	Co(DIM), 5.4 cm^2 glassy carbon plate cathode	62.0 ± 1.0% at 96 h (30 h cumulative CPE)	57.4 ± 0.2% at 96 h (30 h cumulative CPE)	20.0 ± 0.2 at 96 h (30 h cumulative CPE)	59.1 ± 1.9 at 96 h (30 h cumulative CPE)	64.7 ± 0.4 cumulative at 96 h (30 h CPE)
*This work	Secondary effluent (2 mM nitrate concentrated to 54 mM)	Co(DIM), 10 cm^2 graphite serpentine flow field	80.8 at 48 h (8 h cumulative CPE)	62.9 % at 48 h (8 h cumulative CPE	329.0 at 48 h (8 h cumulative CPE	2193.5 at 48 h (8 h cumulative CPE	66.6 cumulative at 48 h (8 h CPE
18	Secondary effluent (2 mM nitrate)	Co(DIM), 64 cm^2 316 SS mesh cathode	70.5 ± 2.7% at 42 h	10-15%	1.9	21	n.r.
19	Agricultural tile drainage (0.27 mM nitrate concentrated to 2.45 mM)	Polyaniline-Co_3O_4-carbon nanotube slurry coated on Ti mesh	n.r.	28%	n.r.	n.r.	n.r.
20	25 mM $NaNO_3$ in 0.1 M Na_2SO_4	Electrodeposited Co on Ti mesh (16 cm^2)	100% at 3 h	43.7%	n.r.	n.r.	n.r.
	Printing wastewater (14.9 mM nitrate)	Electrodeposited Co on Ti mesh (16 cm^2)	100% at 3 h	n.r.	n.r.	n.r.	n.r.
21	*25 mM $NaNO_3$ in 0.5 M Na_2SO_4*	CuO@Cu foam	~100%	49.2%	1846 ± 46	n.r.	n.r.
	Pharmaceutical industry wastewater (31.1 ± 1.1 mM nitrate)	CuO@Cu foam	>96.9%	n.r.	1817 ± 75	n.r.	n.r.
22	Oil refining & chemical catalyst manufacturing wastewater (36.1 ± 0.9 mM nitrate)	Ni foam (1.4 m^2)	95%	n.r.	n.r.	n.r.	n.r.

[23]	*1.12 M KNO_3 in 60 wt% NaOH/KOH*	Ni mesh (100 cm^2), 80 °C	n.r.	70.4%	n.r.	n.r.	n.r.

505 *Equations used to calculate ECaB performance metrics in this work are provided in Section S.5.1.

506

507 Table S6. Efficiency, rate, and energy comparison to literature: TAN production by NO_3RR

ref	Wastewater	Electrode/catalyst (Geometric surface areas)	NO_3RR product	TAN yield (Y_{TAN})	TAN yield rate		TAN production energy consumption
					$\mu g\ N\ cm^{-2} h^{-1}$	$mg\ N\ L^{-1} day^{-1}$	kWh kg-N^{-1}
*This work	Secondary effluent (2 mM nitrate concentrated to 5.8 mM)	Co(DIM), 5.4 cm^2 glassy carbon plate cathode	TAN in 1 M KCl	49.0 ± 2.6% at 96 h (30 h cumulative CPE)	15.7 ± 0.9 at 96 h (30 h cumulative CPE)	46.2 ± 0.8 at 96 h (30 h cumulative CPE)	81.9 ± 3.5 cumulative at 96 h (30 h CPE)
*This work	Secondary effluent (2 mM nitrate concentrated to 54 mM)	Co(DIM), 10 cm^2 graphite serpentine flow field	TAN in 1 M KCl	82.5 at 48 h (8 h cumulative CPE)	319.6 at 48 h (8 h cumulative CPE)	2130.6 at 48 h (8 h cumulative CPE)	67.2 cumulative at 48 h (8 h CPE)
18	Secondary effluent (2 mM nitrate)	Co(DIM), 64 cm^2 316 SS mesh cathode	TAN in secondary effluent	n.r.	n.r.	n.r.	n.r.
19	Agricultural tile drainage (0.27 mM nitrate concentrated to 2.45 mM)	Polyaniline-Co_3O_4-carbon nanotube slurry coated on Ti mesh	TAN in 0.1 M NaCl	n.r.	89.0	n.r.	159.1 for NO_3RR (251.3 including extraction)
20	*25 mM $NaNO_3$ in 0.1 M Na_2SO_4*	Electrodeposited Co on Ti mesh (16 cm^2)	TAN in $NaNO_3$ and 0.1 M Na_2SO_4	n.r.	n.r.	n.r.	n.r.
	Printing wastewater (14.9 mM nitrate)	Electrodeposited Co on Ti mesh (16 cm^2)	TAN in printing wastewater	n.r.	n.r.	n.r.	n.r.
21	25 mM $NaNO_3$ in 0.5 M Na_2SO_4	CuO@Cu foam	TAN in $NaNO_3$ and 0.5 M Na_2SO_4	n.r.	n.r.	n.r.	n.r.
	Pharmaceutical industry wastewater (31.1 ± 1.1 mM nitrate)	CuO@Cu foam	TAN in $NaNO_3$ and 0.5 M Na_2SO_4	n.r.	n.r.	n.r.	n.r.
22	Oil refining & chemical catalyst manufacturing wastewater (36.1 ± 0.9 mM nitrate)	Ni foam (1.4 m^2)	TAN in manufacturing wastewater	n.r.	n.r.	n.r.	n.r.

[23]	*1.12 M KNO_3 in 60 wt% NaOH/KOH*	Ni mesh (100 cm^2), 80 °C	TAN in 60 wt% NaOH/KOH	n.r.	11494	n.r.	83.4 for NO_3RR (does not include extraction)

*Equations used to calculate ECaB performance metrics in this work are provided in Section S.5.1.

509 Table S7. Efficiency, rate, and energy comparison to literature: TAN recovery

ref	Wastewater	Recovery mechanism	Recovered product	TAN recovery efficiency ($\eta_{TAN\ Recovery}$)	TAN recovery rate		TAN recovery energy consumption
					$\mu g\ N\ cm^{-2} h^{-1}$	$mg\ N\ L^{-1} day^{-1}$	kWh kg-N^{-1}
*This work	Secondary effluent (2 mM nitrate concentrated to 5.8 mM)	Electrochemical basification + Membrane stripping (5.4 cm^2 membrane area)	$(NH_4)_2SO_{4,aq}$ in 0.1 M $H_2SO_{4,\ aq}$	91.0 ± 2.1% at 96 h (*Overall N recovery: 42.6 ± 1.4%)	6.0 ± 0.2 at 96 h	18.1 ± 0.2 at 96 h	90.0 ± 2.7 at 96 h (cumulative)
*This work	Secondary effluent (2 mM nitrate concentrated to 54 mM)	Electrochemical basification + Membrane stripping (5.4 cm^2 membrane area)	$(NH_4)_2SO_{4,aq}$ in 0.1 M $H_2SO_{4,\ aq}$	22.8% at 48 h (*Overall N recovery: 11.0%)	45.8 at 48 h	169.6 at 48 h	295.3 at 48 h (cumulative)
18	Secondary effluent (2 mM nitrate)	Electrochemical basification + Membrane stripping (64 cm^2 membrane area)	$(NH_4)_2SO_{4,aq}$ in 0.1 M $H_2SO_{4,\ aq}$	Overall N recovery: 53.6 ± 2.8%	1.3	15.9	340 ± 30 (cumulative)
19	Agricultural tile drainage (0.27 mM nitrate concentrated to 2.45 mM)	n/a					
20	*25 mM $NaNO_3$ in 0.1 M Na_2SO_4*	Electrochemical basification + Membrane stripping (16 cm^2 membrane area)	$(NH_4)_2SO_{4,aq}$ in 1 M $H_2SO_{4,\ aq}$	Overall N recovery: 83.8% at 3 h	n.r.	n.r.	155
	Printing wastewater (14.9 mM nitrate)	Electrochemical basification + Membrane stripping (16 cm^2 membrane area)	$(NH_4)_2SO_{4,aq}$ in 1 M $H_2SO_{4,\ aq}$	Overall N recovery: 86% at 3 h	n.r.	n.r.	n.r.
21	25 mM $NaNO_3$ in 0.5 M Na_2SO_4	Electrochemical basification + Membrane stripping (4 cm^2 membrane area)	$(NH_4)_2SO_{4,aq}$ in acidified 0.5 M $Na_2SO_{4,\ aq}$	Overall N recovery: ~100%	733 ± 42	n.r.	140.6 ± 13.7
	Pharmaceutical industry wastewater (31.1 ± 1.1 mM nitrate)	Electrochemical basification + Membrane stripping (4 cm^2 membrane area)	$(NH_4)_2SO_{4,aq}$ in acidified 0.5 M $Na_2SO_{4,\ aq}$	n.r.	916 ± 27	n.r.	n.r.
22	Oil refining & chemical catalyst manufacturing	n/a					

	wastewater (36.1 ± 0.9 mM nitrate)						
[23]	*1.12 M KNO_3 in 60 wt% NaOH/KOH*	Carrier gas stripping	$NH_{3,(aq)}$, NH_4HCO_3, $(NH_4)_2SO_4$	~100%	n.r.	n.r.	n.r.

*Equations used to calculate ECaB performance metrics in this work are provided in Section S.5.

References

1 Solubility product constants, https://www.engineeringtoolbox.com/solubility-product-equilibrium-constant-ionic-solution-salt-Ksp-d_1952.html, (accessed July 6, 2023).

2 A. Atrashkevich, A. S. Fajardo, P. Westerhoff, W. S. Walker, C. M. Sánchez-Sánchez and S. Garcia-Segura, *Water Research*, 2022, **225**, 119118.

3 S. Xu, D. C. Ashley, H.-Y. Kwon, G. R. Ware, C.-H. Chen, Y. Losovyj, X. Gao, E. Jakubikova and J. M. Smith, *Chem. Sci.*, 2018, **9**, 4950–4958.

4 A. Ch. Lazanas and M. I. Prodromidis, *ACS Meas. Sci. Au*, , DOI:10.1021/acsmeasuresciau.2c00070.

5 A. J. Bard and L. R. Faulkner, *Electrochemical methods: fundamentals and applications*, Wiley, New York, 2nd ed., 2001.

6 J. Guo, P. Brimley, M. J. Liu, E. R. Corson, C. Muñoz, W. A. Smith and W. A. Tarpeh, *ACS Sustainable Chem. Eng.*, , DOI:10.1021/acssuschemeng.3c01057.

7 W. J. Cole, B. A. Frew, P. J. Gagnon, J. Richards, Y. Sun, R. M. Margolis and M. A. Woodhouse, *SunShot 2030 for Photovoltaics (PV): Envisioning a Low-cost PV Future*, 2017.

8 H. T. Kim and W. J. Frederick, *J. Chem. Eng. Data*, 1988, **33**, 177–184.

9 K. S. Pitzer, *A thermodynamic model for aqueous solutions of liquid-like density*, Lawrence Berkeley Lab., CA (USA), 1987.

10 K. S. Pitzer, *Activity Coefficients in Electrolyte Solutions*, CRC Press, 2018.

11 K. S. Pitzer and J. J. Kim, *J. Am. Chem. Soc.*, 1974, **96**, 5701–5707.

12 USDA ERS - Fertilizer Use and Price, https://www.ers.usda.gov/data-products/fertilizer-use-and-price.aspx, (accessed January 26, 2023).

13 *Science of The Total Environment*, 2017, **603–604**, 445–452.

14 Y. Wang, A. Xu, Z. Wang, L. Huang, J. Li, F. Li, J. Wicks, M. Luo, D.-H. Nam, C.-S. Tan, Y. Ding, J. Wu, Y. Lum, C.-T. Dinh, D. Sinton, G. Zheng and E. H. Sargent, *J. Am. Chem. Soc.*, 2020, **142**, 5702–5708.

15 W. A. Tarpeh, J. M. Barazesh, T. Y. Cath and K. L. Nelson, *Environ. Sci. Technol.*, 2018, **52**, 1453–1460.

16 A. Kogler, N. Sharma, D. Tiburcio, M. Gong, D. M. Miller, K. S. Williams, X. Chen and W. A. Tarpeh, *ACS Environ. Au*, , DOI:10.1021/acsenvironau.3c00058.

17 A. Kogler, N. Sharma, D. Tiburcio, M. Gong, D. M. Miller, K. S. Williams, X. Chen and W. A. Tarpeh, 2023.

18 M. J. Liu, D. M. Miller and W. A. Tarpeh, *Environ. Sci. Technol. Lett.*, 2023, **10**, 458–463.

19 K. Kim, A. Zagalskaya, J. L. Ng, J. Hong, V. Alexandrov, T. A. Pham and X. Su, *Nat Commun*, 2023, **14**, 823.

20 J. Gao, N. Shi, X. Guo, Y. Li, X. Bi, Y. Qi, J. Guan and B. Jiang, *Environ. Sci. Technol.*, 2021, **55**, 10684–10694.

21 J. Gao, N. Shi, Y. Li, B. Jiang, T. Marhaba and W. Zhang, *Environ. Sci. Technol.*, 2022, **56**, 11602–11613.

22 W. Zheng, L. Zhu, Z. Yan, Z. Lin, Z. Lei, Y. Zhang, H. Xu, Z. Dang, C. Wei and C. Feng, *Environ. Sci. Technol.*, 2021, **55**, 13231–13243.

23 Y. Chen, P. Ammari-Azar, H. Liu, J. Lee, Y. Xi, M. J. Castellano, S. Gu and W. Li, *EES. Catal.*, 2023, **1**, 504–515.